

# Deep learning for quality control of surface physiographic fields using satellite Earth observations

Tom Kimpson,<sup>1</sup> Margarita Choulga,<sup>2</sup> Matthew Chantry,<sup>2</sup> Gianpaolo Balsamo,<sup>2</sup> Souhail Boussetta,<sup>2</sup> Peter Dueben,<sup>2</sup> and Tim Palmer<sup>1,1</sup> Department of Physics, University of Oxford, Oxford, UK,<sup>2</sup> Research Department, European Centre for Medium-Range Weather Forecasts (ECMWF), Reading, UK<sup>Kimpson et al.</sup>, Tom Kimpson<sup>1</sup>, Margarita Choulga<sup>2</sup>, Matthew Chantry<sup>2</sup>, Gianpaolo Balsamo<sup>2</sup>, Souhail Boussetta<sup>2</sup>, Peter Dueben<sup>2</sup>, and Tim Palmer<sup>1</sup>

<sup>1</sup>Department of Physics, University of Oxford, Oxford, UK

<sup>2</sup>Research Department, European Centre for Medium-Range Weather Forecasts (ECMWF), Reading, UK

Correspondence: Tom Kimpson (tom.kimpson@physics.ox.ac.uk)

**Abstract.** About 2/3 of all densely populated areas (i.e. at least 300 inhabitants per  $\text{km}^2$ ) around the globe are situated within a 9 km radius of a permanent waterbody (i.e. inland water or sea/ocean coast), since inland water sustains the vast majority of human activities. Water bodies exchange mass and energy with the atmosphere and need to be accurately simulated in numerical weather prediction and climate modelling as they strongly influence the lower boundary conditions such as skin temperatures, turbulent latent and sensible heat fluxes and moisture availability near the surface. All the non-ocean water (resolved and sub-grid lakes and coastal waters) are represented in the A purposely built deep learning algorithm for the Verification of Earth-System ParametRisation (VESPER) is used to assess recent upgrades of the global physiographic datasets underpinning the quality of the Integrated Forecasting System (IFS) of the European Centre for Medium-Range Weather Forecasts (ECMWF) model, by the Fresh-water Lake (FLake) parametrisation, which treats  $\sim 1/3$  of the land. It is a continuous enterprise to update the surface parametrization schemes and their input fields to better represent small-scale processes. It is, however, difficult to quickly determine both the accuracy of an updated parametrisation, and the added value gained for the purposes of numerical modelling. The aim of our work is to quickly and automatically assess the benefits of an updated lake parametrisation making use of a neural network regression model trained to simulate satellite observed surface skin temperatures. We deploy this tool to determine, which is used both in numerical weather prediction and climate reanalyses. A neural network regression model is trained

to learn the mapping between the surface physiographic dataset plus the meteorology from ERA5, and the MODIS satellite skin temperature observations. Once trained, this tool is applied to rapidly assess the quality of upgrades of the land-surface scheme. Upgrades which improve the prediction accuracy of the machine learning tool indicate a reduction of the errors in the surface fields used as input to the surface parametrisation schemes. Conversely, incorrect specifications of the surface fields decrease the accuracy with which VESPER can make predictions. We apply VESPER to assess the accuracy of recent upgrades to the FLake parametrisation, namely the improved permanent lake cover and the capacity of the permanent lake and glaciers covers as well as planned upgrades to represent seasonally varying water bodies (i.e. ephemeral lakes). We show that for grid-cells where the lake fields have been updated, the prediction accuracy in the land surface temperature improves by 0.45 (i.e mean absolute error difference between updated and original physiographic datasets) improves by 0.37 K on average, whilst for the subset of points where the lakes have been exchanged for bare ground (or vice versa) the improvement is 1.12–0.83 K. We also show that updates to the glacier cover improve further the prediction accuracy by 0.14 K. The inclusion of seasonal water is shown to be particularly effective for grid points which are highly time variable, generally improving the simulation accuracy by  $\sim 1$  K. The neural network regression model has proven to be useful and easily adaptable to assess unforeseen impacts of ancillary datasets, also detecting inappropriate changes of high vegetation to bare ground, which would lead to decreased the skin temperature simulation accuracy

by 0.49 K, proving to be a valuable support to model development 0.22 K. We highlight how neural networks such as VESPER can assist the research and development of surface parametrizations and their input physiography to better represent Earth's surface coupled processes in weather and climate models.

## 1 Introduction

Accurate knowledge of the global surface physiography, including land, water and ice covers, and their characteristics, strongly determines the quality of surface and near-surface temperature simulations in weather and climate modelling. For instance, water bodies exchange mass and energy with the atmosphere and their thermal inertia strongly influence the lower boundary conditions such as skin temperatures, and surface fluxes of heat and moisture near the surface. Globally, there are  $\sim 117$  million lakes - defined as inland water bodies without lateral movement of water - making up around 3.7% of the Earth's land surface Verpoorter et al. (2014) (Verpoorter et al., 2014). Their distribution is highly anisotropic non-uniform, with the majority of lakes located between 45 – 75°N in the Boreal and Arctic regions. Lakes are highly important from the perspective of both numerical weather prediction and climate modelling as part of the EC-Earth model. For the latter, lakes generally influence the global carbon cycle as both sinks and sources of greenhouse gases; the majority of lakes are net heterotrophic, (i.e. over saturated with carbon dioxide, CO<sub>2</sub>), as a result of in lake respiration and so emit carbon into the atmosphere Pace and Prairie (2005); Tranvik et al. (2009) (Pace and Prairie, 2005; Tranvik et al., 2009). Total CO<sub>2</sub> emission from lakes is estimated at 1.25 – 2.30 Pg of CO<sub>2</sub>-equivalents annually DelSontro et al. (2018) CO<sub>2</sub>-equivalents annually (DelSontro et al., 2018), nearly 20% of global CO<sub>2</sub> fossil fuel emissions, whilst lakes account for 9-24 % of CH<sub>4</sub> emissions, the second largest natural source after wetlands Saunois et al. (2020) (Saunois et al., 2020). These rates of greenhouse gas emission are expected to rise further if the eutrophication (i.e. nutrient concentration increase) of the Earth's lentic systems continues. With regards to weather, freezing and melting of the lake surface modifies the radiative and conductive properties and consequently affects the heat (latent, sensible) exchange and surface energy balance Huang et al. (2019); Lu et al. (2020); Franz et al. (2018) (Franz et al., 2018; Huang et al., 2019; Lu et al., 2020). Considering particular examples, over Lake Victoria convective activity is suppressed during the day and peaks at night, leading to intense, hazardous thunderstorms Thiery et al. (2015, 2017) (Thiery et al., 2015, 2017); Lake Ladoga can generate low level clouds which can cause variability in the 2m temperature of up

to 10 K Eerola et al. (2014) (Eerola et al., 2014); the Laurentian Great Lakes can cause intense winter snow storms Vavrus et al. (2013) Notaro et al. (2013) (Notaro et al., 2013; Vavrus et al., 2013). Moreover, as a result of the increased temperatures due to climate change, lakes become more numerous due to the melting of glaciers and permafrost. Additionally, the higher temperatures mean that previously permanent lake bodies become seasonal or intermittent. There is then evidently a huge potential return in the ability to accurately model the location, morphology and properties of lakes in weather and climate models.

The Integrated Forecasting System (IFS) at the European Centre for Medium Range Weather Forecasts (ECMWF) is used operationally for numerical weather prediction and climate modelling. Earth-system modelling in the IFS can be broadly categorised into large-scale and small-scale processes. Large-scale processes can be described by numerically solving the relevant set of differential equations, to determine e.g. the general circulation of atmosphere. Conversely, small-scale processes such as clouds or land-surface processes are represented via parametrisation. Accurate parametrisations are essential for the overall accuracy of the model. For example, the parametrisation of the land surface determines the sensible and latent heat fluxes, providing the lower boundary conditions for the equations of enthalpy and moisture in the atmosphere Viterbo (2002) (Viterbo, 2002).

Lakes are incorporated in Earth-system models via parametrisation. At ECMWF the representation of lakes via parametrisation was first handled by introducing the Fresh water Lake model FLake Mironov (2008) (Mironov, 2008) into the IFS. FLake treats all resolved inland waterbodies (i.e. lakes, reservoirs, rivers which are dominating in a grid-cell) and unresolved or sub-grid water (i.e. small inland waterbodies and sea/ocean coastal waters which are present but not dominating in a grid-cell). Note that lake parameters are also an important part of the FLake model so when we refer in this work to "lake parametrisation" we mean both the model and the parameters Its main drivers (input fields) are lake location and lake mean depth. The broad impact of the FLake model (i.e. areas where it is active) and the important role that waterbodies play in human life can be illustrated by analysing ECMWF maps fields of the fractional land sea mask and the inland waterbody cover alongside maps of the population density field (i.e. inhabitants per km<sup>2</sup>) based on the population count for 2015 from the Global Human Settlement Layers (GHSL), Population Grid 1975-2030 Schiavina et al. (2022); Freire et al. (2016) (Freire et al., 2016; Schiavina et al., 2022) at 9 km horizontal resolution.

Globally FLake is active over 11.1% of the grid-cells, with only 1.2% of them being resolved inland waters (i.e. water covers  $\geq 50\%$  of the grid-cell); considering only non-ocean (i.e. land) land grid-cells, then FLake is active over 32.4%

of the ~~grid cells with only 3.5% of them being resolved waterspoints~~. According to the population data, ~~only 4% of land is densely populated (i.e. 64.5% of densely populated areas (at least 300 inhabitants per km<sup>2</sup>); 64.5% of these areas being~~ are situated within a 9 km radius of a permanent waterbody (i.e. inland water or sea/ocean coast) ~~with half of it (i.e., with~~ 31.2% of densely populated areas) being in the vicinity of at least 1 km<sup>2</sup> waterbody - emphasising how essential waterbodies are in human life. In some regions this role may be even more crucial than in the others. For example, ~~only 2% of the North American region (similar for South American and North Asian regions) is densely populated with in North America~~ 45.7% (33.9% and 37.9% respectively) of the areas being in vicinity of at least 1 km<sup>2</sup> waterbody; for Europe even though it has more of the densely populated areas (~~16% of land is densely populated~~) still 37.4% of the population are in the vicinity of at least a 1 km<sup>2</sup> waterbody; for a rather dry continent like Africa only 5% of land is densely populated with 22.2% of these areas being close to at least ~~are close to~~ a 1 km<sup>2</sup> waterbody; ~~most striking in this sense is in~~ Australia where only 0.5 % of the land is populated, ~~with~~ two thirds of the population ~~living~~ live within 9 km radius of a permanent waterbody of at least 1 km<sup>2</sup>, with the majority of people living on the ocean coast.

It is a continuous enterprise to update the lake parametrization ~~schemes and their input data~~ ~~input~~ fields to better represent small-scale surface processes. It is however challenging to ~~accurately represent lakes in these parametrisations; do it accurately as~~ the majority of lakes which are resolved at a 9km grid spacing have not had their morphology accurately measured, let alone monitored, whilst 28.9% of land and coastal cells are treated for sub-grid (*i.e. covering half or less of a grid cell*) water. When introducing an updated lake representation it is difficult apriori to determine the additional value gained through doing so. There are two key factors here:

- Are the updated fields ~~accurate~~ closer to reality?
- ~~Are~~ Do the updated fields ~~informative~~ increase the accuracy of the model predictions?

The first point is straightforward; we want our ~~parametrisation~~ fields to better represent reality. If the lake depth of some lake is updated from 10m to 100m we want to be sure that 100m is closer to the true depth of the lake. For the second point, even if the updated fields are accurate, are they informative in the sense that they enable us to make more accurate predictions? For instance, the main target of lake parametrization is to reproduce lake surface water temperatures (and therefore evaporation rates). If a ~~lake parametrisation scheme is~~ ~~lake parametrisation input fields are~~ updated to better represent different types of inland waterbodies, the time variability of inland waterbodies and/or the lake morphology fields use more in situ mea-

surements, does this additional information allow for more accurate predictions of the lake surface water temperatures? Is it therefore worthwhile to ~~update the parametrisation in this way~~ ~~spend several person-months to update/create a lake-related field~~? Since the resulting updated fields are ultimately used operationally, it is essential to ensure the accuracy of the fields and prevent any potential degradation or instability of the model. This problem of quickly and automatically ~~verifying~~ ~~checking~~ the accuracy and information gain of updated ~~lake parametrisations~~ ~~lake-related fields~~ is the aim of this work.

Numerical weather prediction and climate modelling are ~~fields~~ ~~domains~~ that are inherently linked with large datasets and complex, non-linear interactions. It is therefore an area that is particularly well placed to benefit from the deployment of machine learning algorithms. At ECMWF, advanced machine learning techniques have been used for parametrisation emulation via neural networks [Chantry et al. \(2021\)](#) ([Chantry et al., 2021](#)), 4D-Var data assimilation [Hatfield et al. \(2021\)](#) ([Hatfield et al., 2021](#)) and the post-processing of ensemble predictions [Hewson and Pillou \(2021\)](#) ([Hewson and Pillou, 2021](#))

Indeed, the early successes of these machine learning methods have led to the development of a 10-year roadmap for machine learning at ECMWF [Düben et al. \(2021\)](#) ([Düben et al., 2021](#)), with machine learning methods looking to be integrated into the operational workflow and machine learning demands considered in the procurement of HPC facilities; ~~the~~ [The](#) ongoing development of novel computer architectures (e.g. GPU, IPU, FGPA) motivates utilizing algorithms and techniques which can efficiently take advantage of these new chips and gain significant performance returns. In this work we will demonstrate a new technique for the Verification of Earth-System Parameterisation (VESPER) based on a deep learning neural network regression model. This tool enables the accuracy of an updated water ~~body parametrization~~ ~~body-related field~~ to be rapidly and automatically assessed, and the added value that such ~~an updated parametrization brings~~ ~~updated fields bring~~ to be quantitatively evaluated.

This paper is organized as follows. In Section 2 we describe the construction of the VESPER tool - the raw input data, the processing steps and the construction of a neural network regressor. In Section 3 we then deploy VESPER to investigate and evaluate updated ~~lake parametrisation~~ ~~lake-related~~ fields. Discussion and concluding remarks are made in Sections ?? 4 and 5 respectively.

## 2 Constructing VESPER

In order to rapidly ~~check the added value and accuracy of a new parametrisation field~~ we will construct assess the

accuracy of new surface physiography fields and if their use in the model increase the accuracy with which we can make predictions, a neural network regression model (VESPER, hereafter) that can learn the mapping between a set of features,  $\bar{x}$ , and targets,  $\bar{y}$  input features  $x$  and targets  $y$  is constructed. In this case the features are the simulated model variables – such as 2m temperature – and the parametrization fields such as the orography or the vegetation, atmospheric and surface model fields (such as 2 metre temperature from ERA5 reanalysis) and the surface physiographic fields (such as orography and vegetation cover used to produce ERA5 reanalysis). See Table 1 for the full list of variables used. The target is the empirical satellite land surface temperature (skin temperature). A trained model LST; skin temperature from MODIS Aqua Day MYD11A1 v006 collection). Once trained, VESPER can then make predictions about the skin temperature given a set of input climate variables – variables (i.e. atmospheric and surface model fields, and surface physiographic fields). In turn, these predictions can then be compared against the true empirical observations and the model observations (i.e. satellite skin temperature) and VESPER’s accuracy evaluated. By varying the number, type and values of the input features to our model VESPER and observing how the accuracy of the model its predictions change, we can explore whether a new or updated feature generally adds value (i.e. increases the prediction accuracy). Some conclusions on if and how features can increase predictability of an actual atmospheric model can be drawn. Moreover, by isolating geographic regions where the predictions get worse with the addition of a new field, we can identify areas where the new field might be less accurate or additional information is needed to describe the area. New/updated surface physiographic fields, areas where these fields might be erroneous or not informative enough can be identified. Due to the inherent stochasticity of training a neural network regression model it is also possible for different models to settle in different local minimums i.e. the network variance/noise. To understand the significance of this, every VESPER configuration was trained four times, each time with a different random seed.

In this section we will now describe the data used for the features and targets in the  $x$  and targets  $y$  in the neural network regression model, how these disparate datasets various data types are joined together, and the details of the neural network model used. VESPER’s construction.

## 2.1 Raw Data

We have two primary sets of

### 2.1 Features and targets

VESPER’s input feature selection (see Table 1) followed (i) permutation importance results for atmospheric and surface

model fields – only fields with the highest importance were chosen; and (ii) expert choice for surface physiographic fields. As a first attempt it was decided to test the current methodology for lake related information, therefore fields that could be most affected by the presence or absence of water were selected, e.g. if lake had to be removed then some other surface had to appear (like bare ground, high or low vegetation, glacier or even ocean) and surface elevation had to change. Changes to the orographic fields will have important influences on temperature through e.g. wind, solar heating, etc. Lake depth changes are similarly important, influencing how a lake freezes, thaws, mixes and its overall dynamical range. VESPER’s target selection followed globally available criteria and the satellite LST is quite well observed globally and with high temporal pattern (daily or even several times a day depending on the location).

## 2.2 Data sources

There are three main sources of data. The first is a selection of surface physiographic fields from ERA5 Hersbach et al. (2020). These can be thought of as our features or inputs to the model (Hersbach et al., 2020) and their updated versions (Choulga et al., 2019; Boussetta et al., 2021; Muñoz Sabater et al., 2021) used as VESPER’s features. As a shorthand we will refer to the original ERA5 physiographic fields as version “V15” and the updated versions as “V20”. The second is land surface temperature – a selection of atmospheric and surface model fields from ERA5, also used as VESPER’s features. The third is day-time LST measurements from the Moderate Resolution Imaging Spectroradiometer (MODIS) GSFC onboard the Aqua satellite. This will be the model target variable (GSFC), used as VESPER’s target variable.

### 2.2.1 Surface physiographic fields

Surface physiographic fields have gridded information of the Earth’s surface properties (e.g. land-use, vegetation type and distribution) and represent surface heterogeneity in the ECLand of the IFS. They are used to compute surface turbulent fluxes (of heat, moisture and momentum) and skin temperature over different surfaces (vegetation, bare soil, snow, interception and water) and then to calculate an area-weighted average for the grid-box to couple with the atmosphere. To trigger all different parametrization schemes the ECMWF model uses a set of physiographic fields, that do not depend on initial condition or forecast step. Most fields are constant; surface albedo is specified for 12 months to describe the seasonal cycle. Dependent on the origin, initial data comes at different resolutions and different projections, and is then first converted to a regular latitude-longitude grid (EPSG:4326) at  $\sim 1\text{km}$  at Equator resolution, and secondly to a required grid and

Atmospheric and surface model fields (11 fields)	<b>Pressure:</b> surface pressure ( $sp$ , Pa), mean sea level pressure ( $msl$ , Pa), <b>Wind:</b> 10 metre U wind component ( $10u$ , m/s), 10 metre V wind component ( $10v$ , m/s), <b>Temperature:</b> 2 metre temperature ( $2t$ , K), 2 metre dewpoint temperature ( $2d$ , K), skin temperature ( $skt$ , K), ice temperature layer 1 (the sea-ice temperature in layer 0-7 cm; $ist1$ , K), ice temperature layer 2 (the sea-ice temperature in layer 7-28 cm; $ist2$ , K), <b>Surface albedo:</b> forecast albedo ( $fal$ , 0-1), <b>Snow:</b> snow depth ( $sd$ , m of water equivalent)
Main surface physiographic fields (19 fields)	<b>Orographic fields:</b> standard deviation of filtered subgrid orography ( $sdfor$ , m), standard deviation of orography ( $sdro$ , m), anisotropy of sub-gridscale orography ( $isir$ , -), angle of sub-gridscale orography ( $anor$ , radians), slope of sub-gridscale orography ( $slor$ , -), geopotential (the gravitational potential energy of a unit mass, at a particular location, relative to mean sea level; at the surface of the Earth, this parameter shows the variation in geopotential (height) of the surface, and is referred to as the orography; $z$ , $m^2 s^{-2}$ ), <b>Land fields:</b> land-sea mask (the proportion of land, as opposed to ocean or inland waters (i.e. lakes, reservoirs, rivers, coastal waters), in a grid-cell; $lsm$ , 0-1), glacier mask (the proportion of a grid-cell covered by glacier; $glm$ , 0-1), <b>Water fields:</b> lake cover (the proportion of a grid-cell covered by inland water bodies; $cl$ , 0-1), lake total depth (the mean depth of inland water bodies; $dl$ , m), <b>Vegetation fields:</b> low vegetation cover ( $cvl$ , 0-1), high vegetation cover ( $cvh$ , 0-1), type of low vegetation ( $tv1$ , -), type of high vegetation ( $tvh$ , -), <b>Soil fields:</b> soil type ( $slt$ , -), <b>Albedo fields:</b> UV visible albedo for direct radiation ( $aluvp$ , 0-1), UV visible albedo for diffuse radiation ( $aluvd$ , 0-1), near IR albedo for direct radiation ( $alnip$ , 0-1), near IR albedo for diffuse radiation ( $alnid$ , 0-1)
Additional surface physiographic fields	Difference for all main surface physiographic fields between V15 and V20 field sets, Difference between V20 static lake cover and monthly varying lake cover (12 maps in total), Saline lake cover (the proportion of a grid-cell covered by saline inland water bodies; units: 0-1)

**Table 1.** Input features used for training the neural network model VESPER; atmospheric model fields (time varying) were kept the same in all simulations, surface physiographic fields (static) were updated when going from the original data based on GlobeCover2009/GLDBv1 (V15 field set) to GSWE/GLDBv3 (V20 field set); in brackets are variables description (where needed), short name (according to the GRIB parameter database) and units.

resolution. Surface physiographic fields used in this work consist of orographic, land, water, vegetation, soil, albedo fields and their difference between initial V15 and updated V20 field sets. See Tables 1 and 2 for the full list of surface physiographic fields and their input sources; for more details see IFS documentation (ECMWF, 2021). As this work is focused on assessing quality of inland water information, main surface physiographic fields are lake cover (derived from land-sea mask) and lake mean depth (see Table 2).

To generate V15 fractional lake cover the GlobCover2009 global map (Bontemps et al., 2011; Arino et al., 2012) is used. This map has a resolution of 300m, corresponds for the year 2009 and covers latitudes 85°N-60°S; corrections outside these latitudes for the polar regions are included separately. In the Arctic no land is assumed, in the Antarctic data from the high-resolution Radarsat Antarctic Mapping Project digital elevation model version 2 (RAMP2; Liu et al., 2015) is used. To generate V20 fractional lake cover more recent higher resolution datasets and updated methods have been used (Choulga et al., 2019). The main data source is the Joint Research Centre (JRC) the Global Surface Water Explorer (GSWE) dataset (Pekel et al., 2016). GSWE is a 30m resolution dataset from Landsat 5,7 and 8, providing information on the spatial and temporal variability of surface water on the Earth since March 1984; here only permanent water was used for lake cover generation as it provided a more accurate inland water distribution on the annual basis (Choulga et al., 2019). Differences between V20 and V15 lake cover fields (see Figure 1) are consistent with the latest global and regional information: (i) increase of lake fraction in V20 compared to V15 over northern latitudes is due to permafrost melt leading to a new thermokarst lake emergence, and due to higher resolution input source and its better satellite image recognition methodologies; (ii) reduction of lake fraction in V20 compared to V15 can be explained with several reasons, like anthropogenic land use change (e.g. Aral Sea, which lies across the border between Uzbekistan and Kazakhstan, has been shrinking at an accelerated rate since the 1960s and started to stabilise in 2014 with an area of 7660 km<sup>2</sup>, 9 times smaller than its size in 1960. GlobCover2009 describes the Aral Sea in 1998, when it was still “only” two times smaller than its 1960 extent, whereas GSWE provides a more up to date map.), use of only permanent water (e.g. Australia, where GlobCover2009 over-represents inland water, as most of these lakes are highly ephemeral, e.g. the endorheic Kati Thanda–Lake Eyre fills only a few times per century. The GSWE updates to this region therefore include only generally permanent water, removing all seasonal and rare ephemeral water.), and change in the ocean and inland water separation algorithm (e.g. north-east of Russia).

To generate V15 lake mean depth (see Figure 2) the Global Lake DataBase version 1 (GLDBv1; Kourzeneva et al., 2012) is used. GLDBv1

has a resolution of 1km and is based on 13000 lakes with in situ lake depth information; outside this dataset all missing data grid-cells (i.e. over ocean and land) have 25 meter value; field aggregation to a coarser resolution is done by averaging. Overestimation of lake depth in summer season can result in strong cold biases and in winter season – lack of ice formation. To generate V20 lake mean depth an updated version GLDBv3 (Choulga et al., 2014) is used. GLDBv3 has the same resolution of ~1km, but is based on an increased number (~1500) of lakes with in situ lake depth information (in addition to bathymetry information over all Finnish navigable lakes), it introduces distinction between freshwater and saline lakes (this information is currently not used by FLake), and suggests the method to assess the depth for lakes without in situ observations using geological and climate type information; field aggregation to a coarser resolution is done by computing the most occurring value. Verification of GLDBv1 and GLDBv3 lake depths against 353 Finnish lake measurements shows that GLDBv3 exhibits a 52 % bias reduction in mean lake depth values compared to GLDBv1 (Choulga et al., 2019). For a further details on lake distribution and depth, the representation of lakes by ECMWF in general see Choulga et al. (2019) and Boussetta et al. (2021).

To expand V15 and V20 lake description (to V15X and V20X respectively) their salinity and time variability information was generated. Even though static permanent water fits better to describe inland water distribution on average all year round, some areas (in Tropics especially) could benefit from having monthly varying information as they have a very strong seasonal cycle, when size, shape and depth of a lake changes over the course of the year, leading to a significant change in modelling the lake temperature response. Similarly, saline lakes behave very differently to fresh water lakes since increased salt concentrations affect the density, specific heat capacity, thermal conductivity, and turbidity, as well as evaporation rates, ice formation and ultimately the surface temperature. These two properties of time variability and salinity are often related; it is common for saline lakes to fill and dry out over the course of the season, which naturally also affects the relative saline concentration of the lake itself. To create a monthly varying lake cover first 12 monthly fractional land-sea masks based on JRC Monthly Water History v1.3 maps for 2010–2020 were created. Since the annual lake maps were created taking into account a lot of additional sources the extra condition on the monthly maps that the monthly water is equal or greater than permanent water distribution from fractional land-sea mask is enforced. To create an inland salt lake cover map, the GLDBv3 salt lake list was used. First, in order to identify separate lakes on ~ 1km resolution lake cover (by “lake cover” we refer the maximum lake distribution based on 12 monthly-varying lake covers), small sub-grid lakes and large lake coasts are masked, i.e. grid-cells that have water fraction

Field category	V15 (initial)	V20 (updated)
Orographic	SRTM30: Shuttle Radar Topography Mission over 60°N-60°S; GLOBE: Global Land One-km Base Elevation Project data over 90-60°N; RAMP2: high-resolution Radarsat Antarctic Mapping Project Digital Elevation Model version 2 data (Liu et al., 2015) over 60-90°S; BPRC: Byrd Polar Research Center over Greenland; IS 50V: Digital Map Database of Iceland over Iceland	As V15, with corrections of erroneous shift
Land	<b>glm:</b> GLCC: Global Land Cover Characteristics version 2.0 over 90°N-90°S except Iceland; Icelandic Meteorological Office (IMO) glacier mask 2013 over Iceland <b>lsm:</b> GlobCover2009 (Bontemps et al., 2011; Arino et al., 2012) over 85°N-60°S; RAMP2: high-resolution Radarsat Antarctic Mapping Project Digital Elevation Model version 2 data (Liu et al., 2015) over 60-90°S; no land assumed over 90-85°N	<b>glm:</b> Norwegian Institute glacier data over Svalbard; Icelandic Meteorological Office (IMO) glacier mask 2017 over Iceland; GIMP: Greenland Ice Mapping Project data (Howat et al., 2014) over Greenland; <b>CryoSat-2</b> satellite glacier data (Slater et al., 2018) over Antarctica (+ manual gap filling); <b>GLIMS:</b> Global Land Ice Measurements from Space data (GLIMS and NSIDC, 2005, updated 2018) over rest of the globe <b>lsm:</b> GSWE: Global Surface Water Explorer (Pekel et al., 2016); <b>glm</b> <b>cl:</b> <i>lsm</i> (ocean is separated at actual resolution by seeding and removing all connected grid-cells, includes the Caspian Sea, the Azov Sea, The American Great Lakes) <b>dl:</b> The Caspian Sea bathymetry; Global Relief Model ETOPO1 (Amante and Eakins, 2009) over the Great Lakes, the Azov Sea; <b>GLDB:</b> Global Lake DataBase version 1 (Kourzeneva et al., 2012) over rest of the globe; 25 meters assumed over missing data grid-cells
Water	<b>cl:</b> <i>lsm</i> (ocean is separated at 1km resolution by upgraded flooding algorithm following Choulga et al. (2019)) <b>dl:</b> GEBCO: General Bathymetric Charts of the Ocean (Weatherall et al., 2015) over the Caspian Sea and the Azov Sea; Global Relief Model ETOPO1 (Amante and Eakins, 2009) over the Great Lakes; <b>GLDB:</b> Global Lake DataBase version 3 (Choulga et al., 2014) over rest of the globe; indirect estimates based on geological origin of lakes (Choulga et al., 2014) over missing data grid-cells	As V15
Vegetation	GLCC: Global Land Cover Characteristics version 1.2. Note that vegetation type represent only dominant type over grid-cell	As V15
Soil	DSMW: FAO/UNESCO Digital Soil Map of the world (FAO, 2003). Note that soil type represent only dominant type over grid-cell	As V15
Albedo	MODIS 5-year climatology (Schaaf et al., 2002); RossThickLiSparseReciprocal BRDF model. Note that Albedo values represent snow free surface albedo	As V15

**Table 2.** List of input datasets for the surface physiographic fields for V15 and V20 field sets. V15X and V20X are identical to V15 and V20 respectively, but with the addition of saline lake cover, and monthly varying lake cover fields.

less than 0.25. Next, number of connected grid-cells in each lake (i.e. connected with sides only) is computed. Then only lakes that have 100 and more connected grid-cells are vectorised, as at ERA5 resolution of  $\sim 31\text{km}$  the grid-cells are quite large and can include a mixture of freshwater and saline lakes. Finally, saline lake vectors are selected by filtering vectors which have no saline lake point from GLDBv3 located – in total 147 large salt lake vectors, which were further used to filter non-saline lakes at 1km resolution lake cover, finally aggregated to  $31\text{km}$  resolution. In the future it is planned to revisit this field and extend the list to include additional data. Note that all non-lake related climate fields such as vegetation cover or orography were updated in V20 field set compared to V15 only in relation to the changing lake fields (i.e. if fraction of lake in the grid cell increased then other fractions like vegetation or bare ground should have increased accordingly).

### 2.2.2 ERA5

Climate reanalyses combine observations and modelling to provide calculated values of a range of climatic variables over time. ERA5 is the fifth generation reanalysis from ECMWF. It is produced via 4D-Var data assimilation of the **atmospheric Integrated Forecast system IFS** cycle 41R2, coupled to a land-surface model (**ECLand**, Boussetta et al., 2021) (**ECLand**, Boussetta et al., 2021), which includes lake parametrization by **FLake** (Mironov, 2008) and an ocean wave model (WAM). The resulting data product provides hourly values of climatic variables across the atmosphere, land and ocean at a resolution of approximately  $31\text{km}$  with 137 vertical sigma levels, up to a height of  $80\text{km}$ . Additionally, ERA5 provides associated uncertainties of the variables at a reduced  $63\text{km}$  resolution via a 10-member Ensemble of Data Assimilations (EDA). **We take In this work ERA5 surface fields on an hourly grain on hourly surface fields at  $\sim 31\text{km}$  resolution on a reduced Gaussian grid, with a highest resolution of  $\sim 31\text{km}$ . Whilst are used. Gaussian grid's spacing between latitude lines is not regular, but lines are symmetrical along the Equator; the number of points along each latitude line defines longitude lines, which start at longitude 0 and are equally spaced along the latitude line. In a reduced Gaussian grid, the number of points on each latitude line is chosen so that the local east-west grid length remains approximately constant for all latitudes (here Gaussian grid is N320, where N is the number of latitude lines between a Pole and the Equator).** The main field used from ERA5 **has extensive vertical coverage across 37 pressure levels, for our purposes we will deal solely with surface fields. The is skin temperature (i.e. temperature of the uppermost surface layer, which has no heat capacity and instantaneously responds to changes in surface fluxes) that forms the interface between the soil and the atmosphere. Skin temperature is a theoretical**

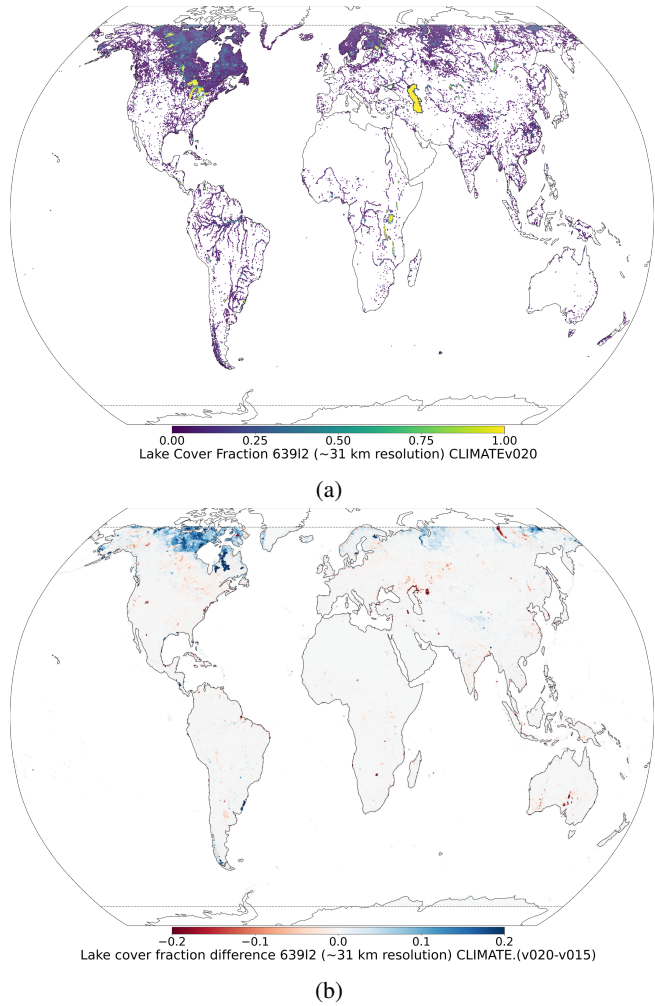


**Figure 1.** At  $\sim 31\text{km}$  resolution (a) V20 fractional lake cover and (b) difference between V20 and V15 lake covers. Over northern latitudes inland water increase in V20 compared to V15 is due to higher resolution input source and its better satellite image recognition methodologies as well as thawing permafrost; inland water reduction in V20 compared to V15 is due to anthropogenic land use changes (e.g. Aral Sea) or due to use of only permanent water (e.g. Australia) which was proven to better represent inland water distribution on annual basis.

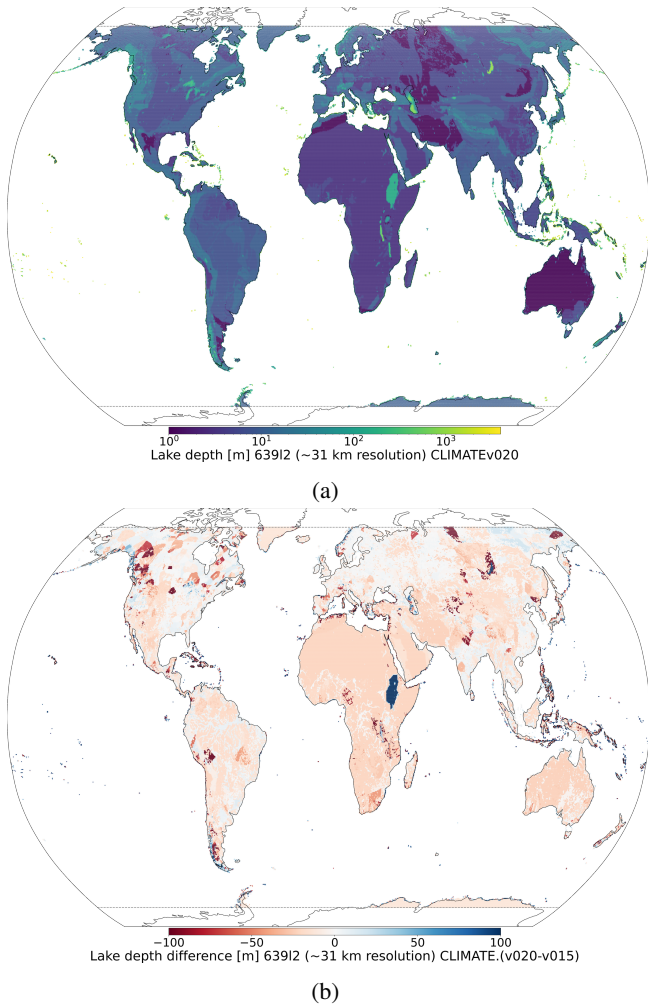


**Figure 2.** At  $\sim 31$  km resolution (a) V15 lake mean depth in meters and (b) difference between V20 and V15 lake mean depths. In general lake mean depth has decreased in V20 compared to V15 due to the use of mean depth indirect estimates based on geological and climate information, instead of default 25 meter value over lakes without any information.

temperature computed by linearizing the surface energy balance equation for each surface type separately, and its feedback on net radiation and ground heat flux is included; for more information see IFS Documentation (2021). 5 ERA5 skin temperature verification against MODIS LST ensemble (i.e. all four MODIS observations were used, namely Aqua Day and Night, Terra Day and Night) over 2003-2018 period showed good correlation between two datasets; errors between ERA5 and MODIS LST ensemble are quite small, i.e. spatially and temporally averaged bias is 10 1.64 K, root-mean square error (RMSE) is 3.96 K, Pearson correlation coefficient is 0.94, and anomaly correlation coefficient is 0.75 (Muñoz Sabater et al., 2021b). ERA5 skin temperature verification against the Satellite Application 15 Facility on Land Surface Analysis (LSA-SAF) product

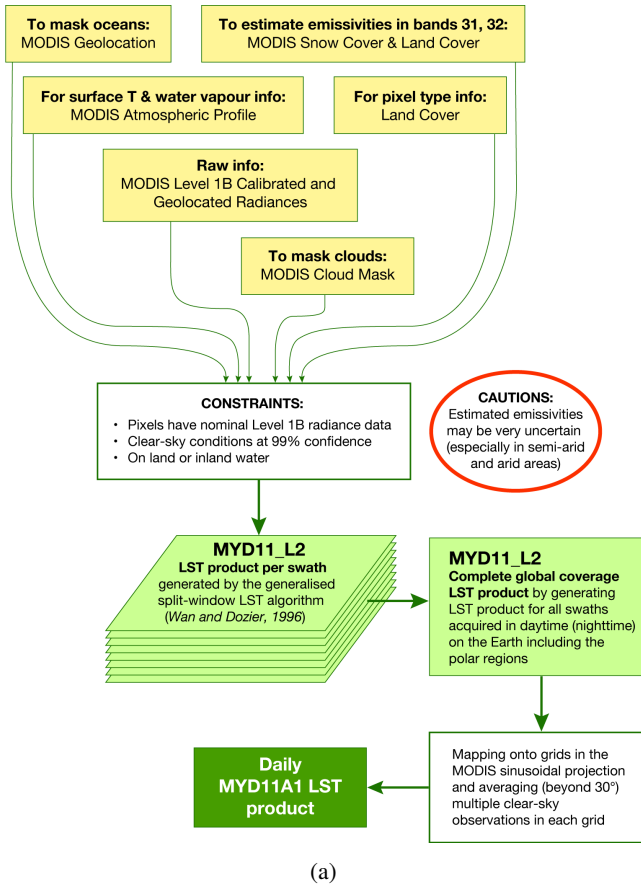
over Iberian Peninsula showed a general underestimation of daytime LST and slightly overestimation at night-time, relating the large daytime cold bias with vegetation cover differences between ERA5 surface physiography fields and the European Space Agency's Climate Change Initiative (ESA-CCI) Land Cover dataset; use of ESA-CCI low and high vegetation cover instead of ERA5 ones led to a complete reduction of the large maximum temperature bias during summer (Johannsen et al., 2019). ERA5 data is obtained via the Copernicus Climate Data Store (CDS, Muñoz Sabater, 2019) (CDS; Muñoz Sabater, 2019).

### 2.2.3 Aqua-MODIS

#### Aqua (Parkinson, 2003)

Aqua (Parkinson, 2003) is a NASA satellite mission which makes up part of the Earth Observing System (EOS). Operating at an altitude of 700 km, with orbital period of 99 minutes, its orbital trajectory passes south to north with an equatorial-crossing times in general of 13:30 30pm. This post-meridian crossing time has led to it sometimes being denoted as EOS PM. Launched in 2002 with an initial expected mission duration of 6 years, Aqua has far exceeded its initial brief and continues to transmit until recently has been transmitting information from 4 of the 6 observation instruments on board. In this work we will concern ourselves with only one of these instruments: MODIS. Here we use information only from MODIS instrument. MODIS can take surface temperature measurements at a spatial resolution of 1 km (the exact grid size is 0.928 km by 0.928 km), operating in the wavelength ranges of between  $\sim 3.7$ – $4.5 \mu\text{m}$  and  $\sim 10.9$ – $12.3 \mu\text{m}$   $\sim 3.7$ – $4.5 \mu\text{m}$  and  $\sim 10.9$ – $12.3 \mu\text{m}$ .

In addition to surface temperature measurements that were used in this work, MODIS can take observations of cloud properties, water vapour, ozone etc., however for this work we will focus exclusively on the surface temperature measurements. We take etc. Here MYD11A1 v006 Wan et al. as our MODIS data product throughout this work which provides daily Land Surface Temperature (LST) (Wan et al., 2015) collection that provides daily LST measurements at a spatial resolution of 1 km on a sinusoidal projection grid SR-ORG:6974, which takes a spherical projection ellipsoid but a WGS84 datum ellipsoid. For our purposes, daily information over several years is needed, so to is exercised. Daily global LST data is generated by first applying a split-window LST algorithm (Wan and Dozier, 1996) on all nominal (i.e. 1 km at nadir) resolution swath (scene) with a nominal coverage of 5 minutes of MODIS scans along the track acquired in daytime, and secondly by mapping results onto integerized sinusoidal projection; for more details see Wan et al. (2015) and Figure 3. Validation of this product was carried out using temperature-based method over different land cover types (e.g. grasslands, croplands, shrublands, woody areas, etc.) in several regions around the globe (i.e. United States, Portugal, Namibia, and China)



(a)

**Figure 3.** A brief step-by-step explanation of the LST algorithm for MYD11A1 v006 collection.

at different atmospheric and/or surface conditions; the best accuracy is achieved over United States sites with RMSE lower than 1.3K (Duan et al., 2019). At large view angles and in semi-arid regions the data product may have slightly higher errors due to rather uncertain classification-based surface emissivities and heavy dust aerosols effects. In addition, the MODIS cloud mask struggles to eliminate all cloud and/or heavy aerosols contaminated grid-cells from the clear-sky ones (LST errors in such grid-cells can be 4-11K and larger). Validation of this product over five bare ground sites in north Africa (in total 12 radiosonde-based datasets validated) showed that mean LST error was within  $\pm 0.6$ K (with exception for one dataset, where mean LST error was 0.8K) and standard deviation of LST errors were less than 0.5K (Duan et al., 2019). In this work to reduce the amount of data daily data over multiple years to store and manipulate, this data product is then prior use LST data is (i) filtered to contain only cloud free data and, and (ii) averaged to a 4km resolution on a regular latitude-longitude grid, EPSG4326. Only 4326 (note that only grid cells which have 8 or more valid observations at 1km resolution are averaged over, otherwise they are classified as missing data).

### 2.3 Joining the data

For a given hour in time we have a selection of To join selected ERA5 data that covers the entire globe at a "low" (31 km) resolution global fields on a reduced Gaussian grid and a strip of MODIS data at "high" (4km) resolution at  $\sim 31$ km resolution (information in UTC, 24 hourly maps per day) with Aqua-MODIS global LST data on a regular grid. We want to be able to join these two datasets in both space and time. That is to say, given a location on the Earth's surface at a particular point in time, what is the observed MODIS LST and the values of corresponding ERA fields? This step is key if we then want to train a model to learn the mapping between ERA5 and MODIS.

In order to proceed it is first latitude-longitude grid at 4km resolution (information in local solar time, 1 map per day), both datasets need to be at the same time space. First it is necessary to determine the absolute time (i.e. UTC) at which the MODIS observations were taken. Since in general all Aqua observations are taken at a 1.30pm local solar time of 13.30, we can relate this straightforwardly, it can be related to a UTC via the longitude of observations as, observation longitude, following Eq. 1:

$$\text{UTC} = \text{Local solar time} - \frac{\text{longitude}}{15}, \quad (1)$$

where the longitude is in degrees, and UTC is rounded to the nearest hour. Naturally, this This conversion is inexact since there is an additional correction as a function of the latitude, but we follow yet recommended by the official MODIS Products User's Guide Wan et al. (2015) which recommends converting between longitude and UTC in this way (Wan et al., 2015); given the short orbital period of Aqua these additional higher order corrections are expected to be typically small. We have also confirmed the accuracy of this and for our purposes can be neglected. Also, the assumption that all Aqua observations are taken at a 1.30pm local solar time of 13.30 (see Fig. ??) was checked (see Figure 4).

The annually averaged mean difference time difference at 31km resolution (i.e. daily differences between local solar time of observations and 1.30pm at 1km resolution were first aggregated to 31km resolution using averaging, and then aggregated in time over a year) is 0.16 or hours or 10 min (MAE is minutes, with mean absolute error (MAE) being 0.46 or hours or 28 min, RMSE is minutes and RMSE being 0.61 or hours or 37 min minutes (current values correspond 70N-70S region year 2019, but confirmed to be approximately identical for each year of 2016-2019 period). Since the ERA5 data has a temporal resolution of an hour, this level of accuracy is sufficient. The conversion generally ERA5 data is hourly, the assumptions inherent to Eq. 1 are sufficiently accurate. Over the poles (i.e. 90-70°N and 70-90°S) satellite sweeps overlap significantly and in general conversion becomes less accurate as one moves towards the poles; on a daily timescale differences at the

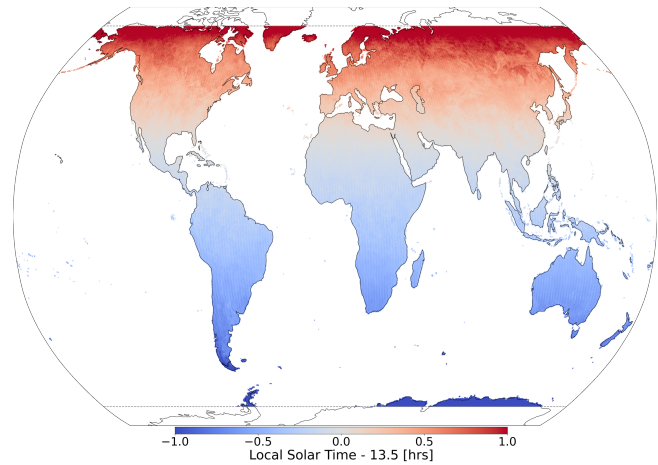
~~poles (daily time differences can reach more than  $\pm 3.5$  hours, for this reason we restrict our analysis throughout this work to grid points with  $|\theta| < 70^\circ$ ), so these areas were not included in the analysis.~~

5 ~~Average (a) Local solar time of MODIS Aqua day, (b) Error relative to the assumed local solar time of 13.30 for the year 2019 at a 31km resolution. The errors are generally sub-hr and grow at greater latitudes. We exclude data with latitudes  $|\theta| < 70^\circ$  and take 13.30 as a constant local solar time.~~

10 ~~Average error in the MODIS LST measurement at a 31km resolution. The raw MODIS data at a 1km resolution provides categorical LST errors with bins  $\leq 1K$ ,  $1-2K$ ,  $2-3K$  and  $> 3K$ . When averaging to 31km resolution we compute a weighted average over the 1km grid cells, where we take the median bin value, and 5K for the  $> 3K$  bin. With the MODIS data converted to an hourly UTC it is then straightforward to match this to the corresponding hour in the ERA dataset. In order to then match in space we select an hour of data and do the following. Once Aqua-MODIS time of observation is converted to UTC, Aqua-MODIS data at  $\sim 4$ km resolution is matched in time and space to ERA5 information in a following way:~~

- 25 1. Take a single **MODIS-Aqua-MODIS** LST observation at a particular point on the MODIS grid;
2. Select ERA5 global hourly map matching **Aqua-MODIS** LST observation time in UTC;
3. Find the nearest point on the ERA5 grid to that MODIS grid point;
4. Repeat ~~for every MODIS observation~~ previous steps for **every Aqua-MODIS observation**;
5. Group **matched data pairs** by the ERA5 grid points, averaging over all the **MODIS-Aqua-MODIS** observations that are associated with each ERA5 point.

40 ~~The result At the end of this process is then for every set of selected ERA5 input fields at a particular point in space and time, we have an empirical LST "observation" which is an average over  $n$  MODIS observations (see e. g. Fig. ??).~~  
 45 ~~We take this averaged observation as the ground truth fields are mapped to a single Aqua-MODIS time of observation and Aqua-MODIS LST data is mapped (i.e. multiple Aqua-MODIS observations could be averaged over, see Figure 5a) to a reduced Gaussian grid at 31km resolution; averaged Aqua-MODIS observations are considered as ground truth (i.e. targets  $y$  that we are) that VESPER is trying to predict. To better understand VESPER's grid-cell results at 31km resolution additional information was computed from Aqua-MODIS, namely (i) total number of valid observations per month and year (see Figure 5a), and (ii) average LST error based on Aqua-MODIS quality~~



55 **Figure 4.** The annually averaged mean time difference of **Aqua-MODIS** and assumed local solar time of 1.30pm for the year 2019 at 31km resolution. Time differences are generally sub-hour and grow at greater latitudes, so data over  $90-70^\circ\text{N}$  and  $70-90^\circ\text{S}$  is excluded.

60 ~~assessment (i.e. quality flag, see Figure 5b). Based on this additional information it can be concluded that areas with sparse number of observations in general have more uncertain LST values; exceptions are Alaska in United States and Anadyrsky District in Russia (area 30° east and west from 180°E around  $70-60^\circ\text{N}$ ), deserts of Australia and Kalahari desert in Namibia, Botswana and South Africa, where majority of vast number of observations have only good or average quality.~~

65 ~~For step (3) in our regression model. Step 2 in the joining pipeline uses process, we use a GPU-accelerated k-nearest neighbours algorithm RAPIDS (v22.04.00), where "nearness" "nearness" on the sphere between two points is measured via the Haversine metric, i.e. the geodesic distance on the sphere between two points:  $H$ , following Eq. 2:~~

$$70 H = 2 \arcsin \left( \frac{d}{2} \right) \sqrt{\sin^2 \left( \frac{\delta\theta}{2} \right) + \cos \theta_1 \cos \theta_2 \sin^2 \left( \frac{\delta\phi}{2} \right)} \quad (2)$$

75 ~~where~~

$$d = \sqrt{\sin^2 \left( \frac{\delta\theta}{2} \right) + \cos \theta_1 \cos \theta_2 \sin^2 \left( \frac{\delta\phi}{2} \right)}$$

70 for two points with coordinate latitudes  $\theta_{1,2}$ , longitudes  $\phi_{1,2}$  and  $\delta\theta = \theta_2 - \theta_1$  and  $\delta\phi = \phi_2 - \phi_1$ .

75 ~~Mean daily number of MODIS observations mapped to each ERA5 data point for 2019. The swath of the **Aqua** satellite is clearly visible, with more observations at more~~

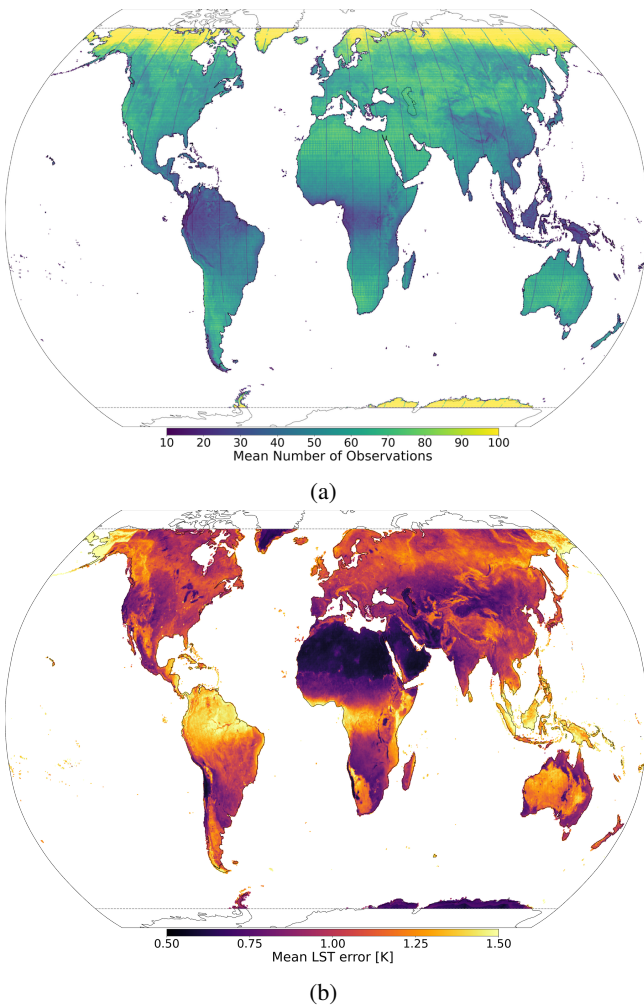


**Figure 5.** For 2019 at  $\sim 31\text{km}$  resolution: (a) Mean daily number of Aqua-MODIS observations mapped to each ERA5 data point. The swath of the Aqua satellite is clearly visible, with more observations over  $70\text{--}60^\circ\text{N}$  and  $60\text{--}70^\circ\text{S}$  areas as Aqua follows a polar orbit, south to north, and with less observations over Equator, complex orography areas (such as the Himalayas, the Andes and the Rocky Mountains), and the Siberian Tundra (due to increased cloud cover); (b) Average error in the Aqua-MODIS LST measurement. The raw Aqua-MODIS data at  $1\text{km}$  resolution provides categorical LST errors with bins  $< 1\text{K}$ ,  $1\text{--}2\text{K}$ ,  $2\text{--}3\text{K}$  and  $> 3\text{K}$ . When averaging to the coarser resolution a weighted average over the  $1\text{km}$  grid-cells is computed, where the median bin value is used, and  $5\text{K}$  for the  $> 3\text{K}$  bin. This information helps to understand that abundant number of observation does not automatically mean high quality of LST (e.g. Australia).

extreme latitudes as Aqua follows a polar orbit, south to north. In addition to the expected increased sparsity of observations at the equator, there are also notably fewer observations in regions of greater orography such as the Himalayas, the Andes and the Rocky Mountains as well as the Siberian Tundra, due to increased cloud cover.

## 2.4 Constructing a regression model

We have our features  $\bar{x}$  and target  $y$  data in a related format. We are now in a position to train a regression model to VESPER is trained to learn the mapping between  $\bar{x}$  and features  $x$  and targets  $y$  (i.e. mapping ERA5 to MODIS), a regression problem. For this purpose we use a sequential a fully-connected neural network architecture, implemented on Tensorflow Abadi et al. (2015) (also known as a multi-layer perceptron), implemented in Tensorflow (Abadi et al., 2016) was used. Whilst more advanced architectures and regression models are available, for our purposes the sequential model is more than sufficient and it the purposes of this work the model is sufficient enough, which exhibits generally fast and dependable convergence. We take as our canonical structure a network where the The networks built have differing number of nodes in the input layer is equal to, depending on the number of training features, a single node in the output layer corresponding to the LST and predictors (see Table 3). For all networks constructed we use 4 hidden layers where the number of nodes in each layer is equal to the half the number of input nodes. For our optimisation scheme we use ADAM Kingma and Ba (2014) and set the learning rate and a layer width is half that of the input layer width. ADAM (Kingma and Ba, 2014) is used as an optimisation scheme, learning rate is set to  $3 \times 10^{-4}$ , and default values for the exponential decay rate for the 1st and 2nd moment estimates take default values of 0.90 and 0.999 are set to 0.900 and 0.999 respectively. The network is not trained for a fixed number of epochs, but instead trained until the validation error reaches a minimum. Techniques for maximising the performance of a network via hyperparameter optimisation are now well established Bischl et al. (2021); Yu and Zhu (2020). However for our purposes we do not try in any meaningful way to tune our hyperparameters, instead just take (Yu and Zhu, 2020; Bischl et al., 2021). However, for the purposes of this work no attempt to tune hyperparameters was made, just some reasonable default values which we judge to be “good enough”. Some shallow were applied which were assumed to be “good enough”. Some exploration of different hyperparameter configuration was undertaken, but for this data the prediction accuracy is mostly independent of the hyperparameter configuration, subject to standard and reasonable hyperparameter choices. Whilst a more advanced automatic hyperparameter optimization method may have enabled slightly more performance to be

squeezed out of the model higher performance of VESPER, our ultimate purpose is not to generate the most absolutely accurate prediction possible, but instead to have two predictive models which we can compare. Additionally, as we will see, can be compared. In the result section below it will be shown that the variation in performance due to modifications to the input features input feature modifications is far greater than the variation due to the hyperparameter choices.

With a fully trained network we can then deploy the model to make predictions of the LST over the whole globe. An example of the error in the predicted LST relative to the true MODIS LST, is presented in Figure 6. The model VESPER was trained on a year of selected atmospheric and surface model fields from ERA5 data from 2016 and then made predictions of the LST in for 2016 (see Table 1), certain static version of the surface physiographic fields (see Table 2), and Aqua-MODIS LST for 2016. Once VESPER was fully trained it was used to predict LST over the whole globe for 2019. We can compare the error in the model predictions with the error in the predicted skin temperature that is derived Going forward, as a shorthand we will refer to VESPER trained using the e.g. V15 field set as VESPER\_V15 (in general VM is a field set version and VESPER VM is a VESPER model trained using the fields from the VM field set). See Table 3 for an explicit definition of all the VESPER models. The training and test years were chosen simply as recent, non-anomalous years so that the updated surface physiographic fields could be checked. All VESPER versions are trained with ERA5. It is evident from Figure 6 that the trained model generally enjoys increased accuracy over the fields for 2016 and with main surface physiographic fields from V15 field set. Then depending on the version some or all additional surface physiographic fields (see Table 1) are added. VESPER's predictions can be compared to the initial ERA5 predictions, skin temperatures and actual Aqua-MODIS LST for 2019. Figure 6 shows the mean absolute errors (MAE) globally in the VESPER\_V15 LST predictions, relative to the Aqua-MODIS LST along with the corresponding MAE in the predicted skin temperature from ERA5. We can see that VESPER\_V15 was able to learn corrections to ERA5, especially in the Himalayas and sub-Saharan Africa as well as Australia and the Amazon basin. For this particular example, the mean annual error, averaged over all grid points was Africa as well as Australia and the Amazon basin, leading to the globally averaged MAE reduction for predicted LST; the MAE relative to Aqua-MODIS LST, averaged over all grid points, was 3.9 K for the ERA5 prediction and 3.0 K for the model prediction. This serves as a useful sanity check to give us confidence that the network is performing as expected and gives generally reasonable predictive performance, at least as good if not better than then derived skin temperature predictions from ERA5. More fundamentally, this also indicates that there is some information captured in the input fields to the network

that is not expressed through the current ERA5 reanalysis modelling. This again motivates the development of updated parametrization schemes that better represent small scale processes and better capture this information.

Prediction error relative to MODIS Aqua observations in the land surface temperature ( $\delta K$ ) for 2019, averaged over the year, for (a) Trained Neural Network and (b) ERA5. It can be seen that the network generally outperforms the ERA5 predictions, which generally struggles in regions with complex surface fields such as the Himalayas (lots of orography) sub-Saharan Africa (lots of vegetation) and the Amazon Basin (lots of water + vegetation). In contrast the network demonstrates generally good performance, with some drop off in the Himalayas and the eastern cost of Australia, but still outperforming ERA5.

### 3 Evaluating Updated Lake Fields

As discussed, at ECMWF parametrised lake representation in the IFS is handled by FLake. The primary physiographic dataset used in the IFS to generate the lake parameters is the GlobCover2009 global map Bontemps et al. (2011) Arino et al. (2012). This map has a resolution of 300m and covers latitudes from 60°S to 85°N; corrections outside this latitude band for the polar regions and Iceland are included separately. In the Arctic no land is assumed, whilst in the Antarctic data from version 2 of the Radarsat Antarctic Mapping Project (RAMP2) digital elevation model (DEM) is used Liu et al. (2015). For Iceland, data from the Digital map database of Iceland (IS-50V) is used.

More recently, new datasets and methods for updating the lake fields for the IFS have been proposed Choulga et al. (2019). These new datasets include the Global Surface Water Explorer (GSWE) dataset from the Joint Research centre (JRC) Pekel et al. (2016). GSWE is a 30m resolution dataset from Landsat 5,7 and 8, providing information on the spatial and temporal variability of surface water on the Earth since March 1984. This then allowed for particular geographical regions to be updated with more up-to-date, high resolution data, providing additional information that is not captured by GlobCover2009. Whilst multiple lake areas were updated based on this new data, particularly noteworthy regions include:

- **Aral Sea.** The Aral Sea lies across the border between Uzbekistan and Kazakhstan and was at one point the 4th largest lake in the world. However, the Aral Sea has long been shrinking, at an accelerated rate since the 1960s. It started to stabilise in 2014 with an area of  $7660\text{ km}^2$ , 9 times smaller than its size in 1960, and its eastern basin is now known as the Aralkum Desert. The water map from GlobCover2009 describes the Aral Sea in 1998, when it was still "only" 2 times smaller than its 1960 extent, whereas GSWE provides a more up-to-date map.

– **Australia.** GlobCover2009 over-represents inland water in Australia, which generally has a huge number of lakes. However, some of these lakes are highly ephemeral; the endorheic Kati Thanda Lake Eyre fills only a few times per century. The GSWE updates to this region therefore include only generally permanent water, removing all seasonal and rare ephemeral water.

The lake depth is not specified by GlobCover2009/GSWE, instead being described by the Global Lake DataBase (GLDB) Kourzeneva et al. (2012). Lake depth is recognized as being an important field in the IFS, since over estimates can result in strong cold biases in hotter seasons or else a lack of ice formation. Under the program to continuously update the parametrisation schemes, recently the original version of the dataset, GLDBv1, with coarse resolution aggregation technique MEAN, has been superseded by GLDBv3 Choulga et al. (2014), with coarse resolution aggregation technique MODE. GLDBv3 increases the total number of lakes with in situ information by  $\sim 1500$ , introduces a depth distinction between freshwater and saline lakes, and updates the method by which the lake depth is calculated based on climate type and geological origins. Consequently, whilst the updated fields when going from GlobCover2009 to GSWE applied at particular geographic regions, the lake depth field is generally updated globally. Verification of the updated lake depth fields against 353 lakes in Finland shows that GLDBv3 exhibits a 52% bias reduction compared to GLDBv1 Choulga et al. (2019). For a thorough discussion of the upgraded lake fields, the lake depth, and the representation of lakes generally by ECMWF we refer the reader to Choulga et al. (2019); Boussetta et al. (2021): 3.0K for VESPER V15.

This distinction between the original lake maps based on GlobCover2009 and GLDBv1 data and the updated lake maps which have been corrected using GSWE and GLDBv3 data provides an ideal test bed to deploy and demonstrate our tool. Can we use VESPER to evaluate the added value of these new fields?

## 2.1 V15 vs V20

In order to ascertain the accuracy and information content of the updated lake fields we will proceed as follows. We will train two permutations of the regression model, one where the

By comparing the accuracy of the predictions of the two models we can then discern the value gained from updating these static surface fields.

There is an inherent noise in the regression model due to the stochasticity of the network; training the model twice with the same architecture, inputs and parameters can find two different minima. Moreover, for the majority of the globe the lake fields have not been updated, since there are no lakes there! By inspecting the predictions at a grid point where the

fields have not been updated in going from V15 to V20 we obviously don't learn anything, instead just measuring the intrinsic model noise, i.e. the different optimisation minima discovered by the model. By comparing two models with the same network structure, trained on the same data, we estimate the noise bias to be 0.04 K over all grid points. Instead we want to restrict our analysis to As the focus of this study is lake-related fields, and lakes occupy only 1.8% of the Earth's surface and are distributed very heterogeneously (Choulga et al., 2014), analysis of the results was restricted to areas where there have been a significant changes in the fields. More quantitatively, we consider a surface lake physiographic fields. By "significant change" to be we mean a change in any of the surface field when going from V15 to V20 of  $\geq 0.1$  (and to V15X or V20X) of  $\geq 10\%$  ( $\geq 0.1$  for fractional fields of  $\geq 10\%$  for non-fractional quantities). So for example, if the field for the lake cover ( $cl$ ) which describes the fraction of the grid box which is classified as a lake changes); for example if lake or vegetation cover changed from 0.1 in V15 to 0.3 in V20 this would be classified as a significant change. Similarly, if the lake depth a non-fractional quantity changes from 10m to 20m, this would also be a significant change. Naturally the choice of  $\geq 10\%$  is a somewhat arbitrary tolerance field set this change is classified as significant. The choice of  $\geq 10\%$  as a significance cut-off, but it balances the was adopted as it proved to be a good trade off between having a sufficient number of grid points to inspect and the strength of the effect of changing the input field. As the tolerance increases we isolate points where the fields have been changed more severely, but have fewer points, cut-off % increases less points are selected, albeit with more severe changes to their surface fields, whereas when the tolerance decreases we have more points but it is cut-off % decreases more points are selected but it becomes more difficult to disentangle the change in the prediction accuracy from the model noise. Alternative tolerances VESPER's training noise (training noise is discussed below). Alternative cut-off % were briefly explored, but our conclusions are conclusions of the results remained broadly unchanged.

Grid points All grid-cells selected for the analysis can be classified according to how the surface fields are updated when going from V15 to V20. We will examine 3 illustrative categories (note that categories represent a systematic and consistent update across multiple related fields, and do not include any restrictions on other surface fields apart the ones mentioned):

– **Lake Updates.** The change in the lake cover  $cl$  and lake depth  $dl$  are significant, but the changes in ocean and glacier  $glm$  fractions are not. This corresponds to grid boxes where inland grid-cells where lakes have been added or removed. We will also use Lake-Ground Updates is a sub-category Lake-Ground-Updates where we have the where additional constraint that the

Model	ERA5 atmospheric and surface fields	Main surface physiographic fields, V15	Main surface physiographic fields, V20	Additional surface physiographic fields
VESPER_V15	✓	✓	-	-
VESPER_V15X	✓	✓	-	✓
VESPER_V20	✓	✓	✓	-
VESPER_V20X	✓	✓	✓	✓

Table 3. List of input files for different VESPER versions. c.f. Table 1

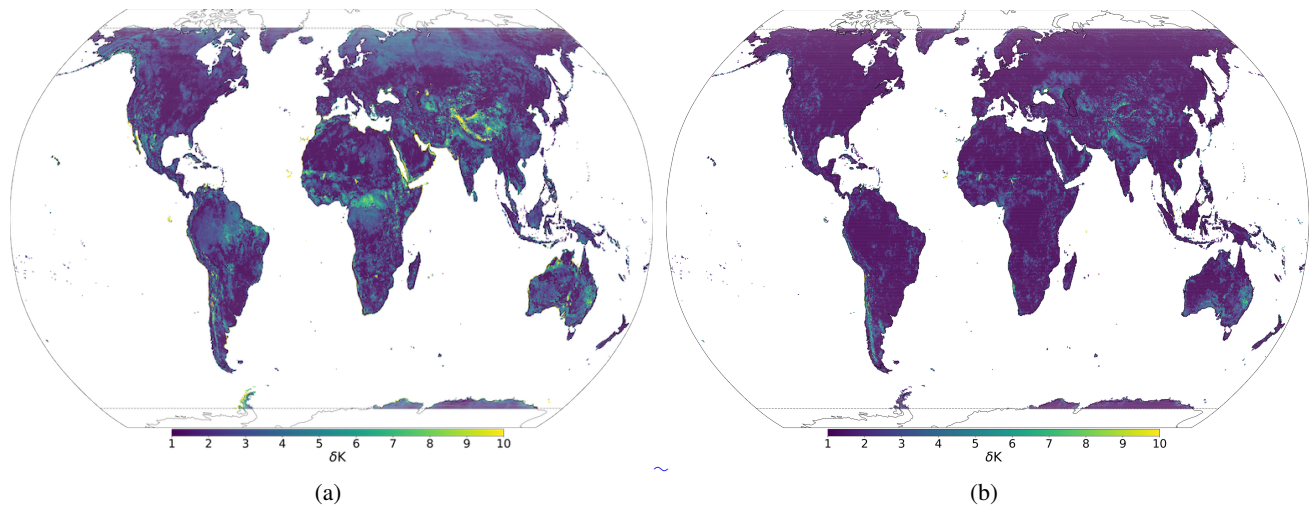


Figure 6. Mean absolute error (MAE,  $\delta K$ ) of LST predictions for 2019 at 31km resolution based on differences between (a) ERA5 skin temperature and Aqua-MODIS LST and (b) between VESPER\_V15 (i.e. VESPER trained with V15 surface physiographic fields) and Aqua-MODIS LST. It can be seen that VESPER\_V15 managed to learn corrections over regions with complex surface fields such as the Himalayas (lots of orography) sub-Saharan Africa (lots of vegetation) and the Amazon Basin (lots of water + vegetation).

change in the high/low vegetation fractions  $cvh/cyl$  are not significant is in place. This then corresponds to the exchange of lakes for bare ground, or vice versa.

- **Vegetation Updates.** The change in the high vegetation fraction  $cvh$  is significant, but the change in lake cover  $cl$  is not significant. This corresponds to grid boxes grid-cells where large features like forests and woodlands have been updated, exchanged for bare ground or low vegetation.
- **Glacier Updates.** The change in the glacier cover  $siHglm$  is significant. This corresponds to any areas where the fraction of glacier ice has been updated.

These categories are naturally broad, and have no restrictions on all of the other features listed in Table ???. For instance, changes to the orography will have important influences on temperature through e. g. wind, solar heating etc. Lake depth is similarly important, influencing how a lake freezes, thaws, mixes and its overall dynamical range. We therefore emphasise that these categories do not correspond to grid points where only the fields that define the categories have been updated, but instead represent a systematic and consistent update across multiple related fields.

We train the model over the entire globe for the year 2016 and make predictions of the land surface temperature for 2019. For each entry in the test set we can determine the prediction accuracy of both the The training of a neural network is inherently stochastic - the same model trained twice with the same data can settle in different local optima and so make different predictions. To make our conclusions robust against this training noise, each VESPER model is in turn trained 4 times. For each MODIS ground truth we then have 4 LST predictions per model. We define the training noise as the standard deviation,  $\sigma$ , in the VESPER predictions for the same input fields i.e. each VESPER VM model will have a corresponding training noise  $\sigma_{VM}$ . To assess the changes of LST predictability due to the use of the updated surface physiographic fields instead of V15 field set (default) we compare the mean absolute error (MAE) between different VESPER models using the simple metric  $\delta_{VM}$ :

$$\delta_{VM} = MAE_{VESPER\_VM} - MAE_{VESPER\_V15} \quad (3)$$

where VM represents one of the field set versions V20, V20X or V15X, and MAE is computed over the whole prediction period of 2019. In turn, the MAE is the error

between the prediction of a VESPER model and V20 models. We will use a simple metric  $\delta_M$  to quantify the difference between an updated model  $M$  and the baseline V15 model the Aqua-MODIS LST, i.e.

$$5 \quad \delta_M = M \text{ prediction error} - \text{V15 prediction error}.$$

$$10 \quad \text{MAE}_{\text{VESPER\_VM}} = \frac{1}{N} \sum_{i=1}^N |\text{LST}_{i,\text{VESPER\_VM}} - \text{LST}_{i,\text{MODIS}}|$$

(4)

So for example,  $\delta_{\text{V20}}$  describes the gain of the V20 model relative to the V15 model for total number of predictions  $N$ , within a given grid-cell classification. A negative  $\delta_{\text{V20}}$  therefore  $\delta_M$  then indicates that the V20 VESPER VM LST prediction is more accurate than the VESPER V15 prediction, and vice versa. The results for the selected grid point categories are presented in Table ??.

### 15 3 Results

#### 3.1 Evaluation of updated lake fields

To understand if there is a way to automatically and rapidly assess the accuracy of updated and/or new surface physiography fields, and if their use in the atmospheric model increase predictability, we can compare the prediction accuracy of different VESPER VM models. Generally VESPER's training noise is confirmed to be smaller than differences in LST predictions by different VESPER configurations, so changes in LST predictability can be meaningfully attributed to the changes in surface physiographic fields. Particular situations where the training noise becomes significant are discussed below.

Category As a first attempt lake-related information is assessed, namely lake cover (and land-sea mask and glacier cover as they are used for lake cover generation) and lake mean depth, that were created from scratch using new up-to-date high-resolution input datasets (see Table 2) for the V20 (and V20X) field set; other surface physiographic fields (see Table 1) were regenerated from the same input sources as in the initial V15 field set, but taking into account that lake related fields were changed. In cases when existing in V15 lake cover water was removed in V20, it could be replaced by any of high or low vegetation, glacier or bare ground. We now analyse the results for each of the 4 categories of grid cell in detail (see Table 4 for the results of each category aggregated over the whole globe).

##### 3.1.1 Category: Lake Updates

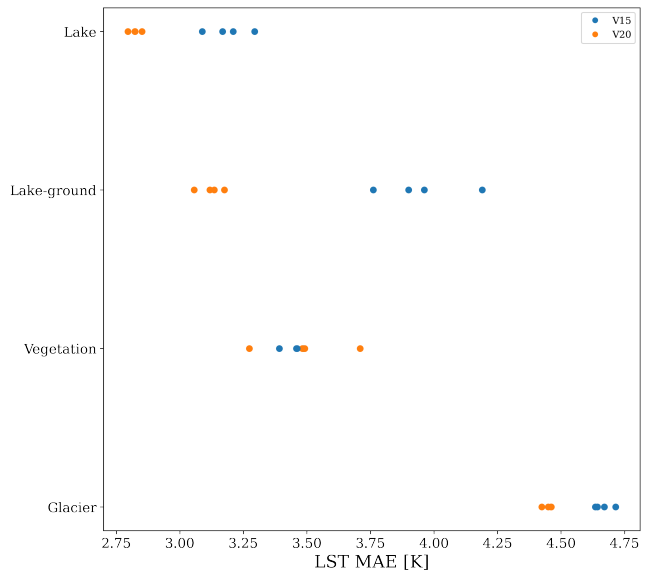
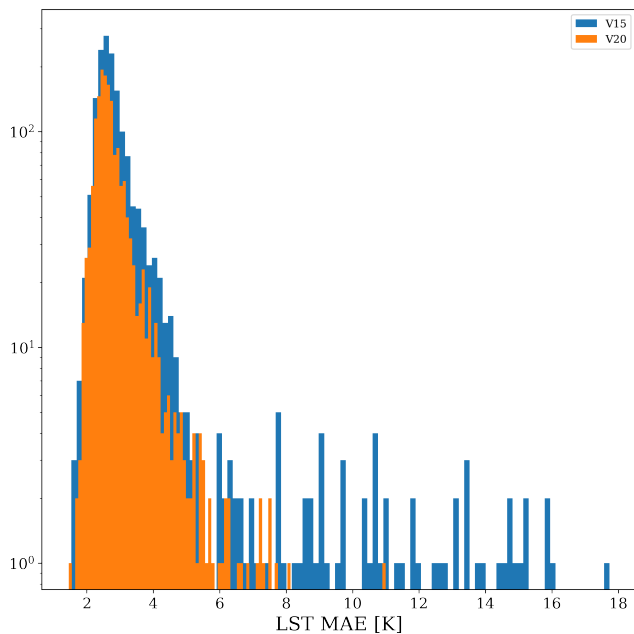


Figure 7. Distribution of prediction errors in the LST, for each of the 4 grid point categories, for each iteration of V15 and V20. For Lake, Lake-ground and Glacier categories the improvement in V20 relative to V15 is much greater than the intrinsic model noise, with all V20 predictions outperforming all V15 predictions. For the Vegetation category the predictions of V15 and V20 are much more noisy and it is difficult to draw any conclusions for the category as a whole.

The Lake Updates category. These points are presented in Figure 9. We can see that there have been significant improvements globally (the mean improvement in the prediction accuracy when using the shows significant improvements in LST predictability if using V20 fields was 0.45 K, over field set instead of V15 – prediction accuracy increased globally (over 1631 grid points), most notably in Australia and the Aral sea. These were two of the major regions that we discussed earlier where in grid-cells) on average by 0.37 K. For the lakes category, the training noise in V20 we have removed the ephemeral water (e.g. for Australia) and corrected lake sizes (e.g. for the Aral sea). By providing this updated information to the model that there is less water than initially thought in these regions, the model can then make more accurate predictions. This is a clear example of a verification of the updated fields was generally small  $\sigma_{\text{V20}} \sim 0.02$  K, with the V15 predictions a little more noisy with  $\sigma_{\text{V15}} \sim 0.07$  K, but this noise is much less than the improvement – it gives us confidence that these new fields are indeed more accurate and are also informative (i.e. predictive) with respect to surface temperatures. as can be seen in Fig. 7 every V20 iteration significantly outperforms every V15 iteration. In Fig. 8 we plot the distribution of the mean LST error (averaged across each of the 4 trained VESPER iterations) for all lake grid points, for both V15 and V20. Evidently the V20 field significantly improve the high

Category	Number of grid cells	$\sigma_{\text{VMS}}, K$				$\delta_{\text{VMS}}, K$		
		V15	V15X	V20	V20X	V15X	V20	V20X
Lake	1631	0.07	0.02	0.02	0.02	-0.20	-0.37	-0.37
Lake-Ground	546	0.15	0.05	0.04	0.06	-0.56	-0.83	-0.84
Vegetation	58	0.04	0.10	0.15	0.21	-0.00	0.04	-0.00
Glacier	1057	0.03	0.08	0.02	0.06	-0.01	-0.22	-0.28

**Table 4.** Globally averaged differences  $\delta_{\text{VMS}}$  between mean absolute error (MAE) of VESPER VM and VESPER V15 LST for 2019 at 31km resolution (where M denotes V15X, V20, V20X field sets) per grid-cell category. Negative  $\delta_{\text{VMS}}$  values indicate an increase of LST predictability due to the use of the updated surface physiographic fields instead of V15 field set (default), positive  $\delta_{\text{VMS}}$  values indicate a decrease in the LST predictability and suggests the presence of erroneous information in the surface physiographic fields. Training noise values,  $\sigma_{\text{VMS}}$ , are generally much smaller than the variance between different VESPER configurations, indicating that changes in LST predictability are mainly due to changes in the surface physiographic fields. The quoted noise is the standard deviation of the prediction errors of Fig. 7.



**Figure 8.** Mean  $\delta$  for Distribution of prediction errors in the V20 model relative to the V15 model across the globe LST for all grid points where all in the lake fields have changed significantly (“Lake Update” Updates category) for VESPER V15 and VESPER V20. Generally Each prediction errors is in turn the updated V20 fields enable average of 4 trained iterations of the VESPER model to make more accurate. The predictions for example in the Aral sea and Australia, indicating that these updated fields of VESPER V20 are informative evidently and accurate. In contrast improvement over VESPER V15, there are some regions where the predictions get worse, especially for example at higher latitudes which is likely due to these being regions where lakes have more complex, time variable behaviour (e.g. freezing/thawing) and MODIS satellite data is sparse e.g. due to clouds. 7 grid points (two are overlaid in sub-Saharan Africa) where the V20 prediction gets notably worse than V15 are highlighted with green circles and discussed in the text large LST errors.

The first category where we see significant improvements is for the

tail behaviour relative to V15, as well as shifting the median of the distribution to lower errors. Particular regions where the V20 physiographic fields notably improved performance were in Australia and the Aral sea (e.g. Fig. 9). These are two major regions where ephemeral lakes were removed and inland water distribution made up-to-date, as discussed in Section 2.2.1. In addition to the areas where there is with a notable improvement in the prediction accuracy, there are also some noteworthy regions where the predictions get worse (got worse (see red points in Fig. Figure 9) suggesting inaccuracies or lack of information in the new fields. We can take a updated surface physiographic fields. A few of the most noteworthy points (highlighted by grid-cells (see red points highlighted with green circles in Fig. 9) in turn Figure 9 and also Figure 11) are:

– **Tanzania Northern India.** There are two grid points here where the V20 predictions are less accurate, both at Lake Natron, in Tanzania, which lies to the south-east of Lake Victoria. One grid point lies on the northern edge of the lake, and the other is more central. For the central point, the This grid-cell lies in the state of Gujarat, India, close to the border with Pakistan. Here  $\delta_{\text{V20}} = +4.21$ , with  $\sigma_{\text{V15}} = 2.54$  and  $\sigma_{\text{V20}} = 0.416$ . The lake fraction was increased from 0.04–0.59 in V15 to 0.39–0.71 in V20. However Lake Natron is a highly saline lake that often dries out, with high temperatures, high levels of evaporation and irregular rainfall. It is a highly complex and variable regime that is not well described by simply increasing the static lake fraction field, and indeed these results suggest that it may in fact be beneficial for the current lake parametrisation scheme to keep the lake fraction low here (see e.g. Fig 10e). Similar arguments apply for the grid point at the northern edge, where the lake fraction has also been increased, along with a small decrease ( $\sim 0.1$ ) in field set, along with the lake depth increase from 2.58m to 3.76m. However, this point lies on a river delta within the Great Raan of Kutch, a large area of salt marshes (see Figure 10a), known for having

highly seasonal rainfall with frequent flooding during the monsoon season and a long dry season. The surface itself also undulates with areas of higher sandy ground known as medaks, with greater levels of vegetation.

and northern edge of Lake Natron, which itself lies to south-east of Lake Victoria, in Tanzania. For both these points VESPER V20 predictions are less accurate than VESPER V15; for the central point ( $\delta_{V20} = +2.45$ ,  $\sigma_{V15} = 0.12$  and  $\sigma_{V20} = 0.81$ , see also Figure 10c) the lake fraction was increased from 0.04 in V15 to 0.39 in V20 was the removal of the water, with field set; for the northern edge point ( $\delta_{V20} = +1.57$ ,  $\sigma_{V15} = 0.13$  and  $\sigma_{V20} = 0.51$ ) the lake fraction decreasing from 0.11 to zero was also increased in V20 comparing to V15 field set along with a small decrease ( $\sim 0.1$ ) in the low vegetation fraction. However, this area in fact has an extensive network of mountain tributaries which feed an ephemeral lake (e.g. Fig. ??). There is therefore likely some surface water for parts of the year, especially during the rainy season, and completely removing all water for this grid point is an overcorrection. Lake Natron is a highly saline lake that often dries out, with high temperatures, high levels of evaporation and irregular rainfall. It is a highly complex and variable regime that is not well described by simply increasing the fraction of permanent fresh water, and indeed results suggest that with current lake parametrization scheme it may be beneficial to keep the lake fraction low or introduce extra descriptor, e.g. salinity.

– **Northern India/Algeria.** This grid point lies in the state of Gujarat, close to the border with Pakistan. The lake fraction  $cl$  was increased from 0.59 to 0.71 and the lake depth  $dl$  increased from 2.58m to 3.76m. That is Algeria, at the northern edge of the Chott Felhrir, an endorheic salt lake ( $\delta_{V20} = +2.20$ , the  $\sigma_{V15} = 0.41$  and  $\sigma_{V20} = 0.49$ ). Similar to the Great Salt Lake Desert, the lake fraction was completely removed from 0.33 in V15 to 0.0 in V20 corrections suggest that there should be a larger degree of lake cover in this grid box. However, this point appears to lie on a river delta within the Great Raan of Kuteh, a large area of salt marshes (Fig. 10a). This area is known to have highly seasonal rainfall, with frequent flooding during the monsoon season and a long dry season. The surface itself also undulates with areas of higher sandy ground known as medaks, with greater levels of vegetation. It is evidently a complex and . However, Chott Felhrir goes through frequent periods of flooding where the lake is filled by multiple large wadi, and corresponding dry periods where the lake becomes a salt pan. As with the Great Salt Lake Desert it is also a highly variable, complex area that may require additional consideration of the salinity and the seasonality.

– **Lake Chad** This grid point contains Lake Chad, a freshwater endorheic lake in the central part of the Sahel ( $\delta_{V20} = +1.74$ ,  $\sigma_{V15} = 0.33$  and  $\sigma_{V20} = 0.98$ ). Here the lake fraction was modestly reduced from 0.63 to

– **Australia.** This grid-cell lies in South Australia and contains Lake Blanche. In going from V15 to It is evidently a complex and highly time variable area and additional static fraction of fresh water provided via V20 all water was removed, with the lake fraction decreasing from 0.44 to 0 and the lake depth reduced from 5.5m to 1m. This water is then replaced with vegetation; the low vegetation fraction  $cl$  increasing from 0.53 to 0.97. Whilst the removal of ephemeral water is generally accurate for Australia, for this grid point it causes the V20 predictions to become worse. Lake Blanche is a salt lake that lies within a wetlands system and so will retain some surface water which will influence the temperature response. The lake itself also lies below sea level, but the orography fields in V15 or V20 do not reflect this. Satellite imagery (e.g. Fig ??) suggests that the area surrounding Lake Blanche is also fairly devoid of any obvious vegetation. The V20 description of a completely dry region covered short grass (low vegetation) is then insufficiently accurate, and results in worse predictions field set is not sufficient.

– **Salt Lake City, North America.** This grid point lies . This grid-cell lies within the Great Salt Lake Desert, just to the west of the Great Salt Lake, Utah, within the Great Salt Lake Desert. All water US. Predictions of VESPER V20 are worse than VESPER V15, with  $\delta_{V20} = +2.91$  ( $\sigma_{V15} = 0.26$  and  $\sigma_{V20} = 0.92$ ). Whilst the training noise is significant here, it is less than the  $\delta_{V20}$  value, and we can see from Fig 11 that the VESPER V20 predictions consistently underperform the VESPER V15 predictions. The lake fraction was completely removed when going from from over 0.50 in V15 to 0.00 in V20 ( $cl$  from  $\gtrsim 0.5$  to 0). The field set, meaning that the grid-cell is fully covered with bare ground in V20 model then treats this region simply as bare ground field set. Whilst this area primarily is bare ground, satellite imagery also suggests the presence of a presumably highly saline lake (Fig 10b). This region also see Figure 10b); in addition area has a large degree of orography and high elevation ( $\sim 1300$  m) which will also further complicate  $\sim 1300$ m) which probably further complicates the surface temperature response. Again, a more accurate description that accounts for the seasonality of the surface water and the salinity is necessary here.

– **Afghanistan/Tanzania.** This grid point lies in the south west of Afghanistan, close to the border with Iran. The only notable change when updating from There are two grid-cells of interest at the centre

0.47. However, Lake Chad is again a highly time variable area and the additional static information provided via the regime with seasonal droughts and wet seasons. It is a marshy wetland area but the vegetation fractions in both V15 and V20 fields is either not accurate or not predictive/informative enough in such a variable regime here are zero. Satellite imagery also shows a large fraction of the surface covered by water and vegetation (Figure 10e).

– **Egypt Al Fashaga** This grid point lies in the south of Egypt, to the west of the River Nile. Again, all water has been removed from this region, with a disputed region between Sudan and Ethiopia called Al Fashaga, close to a tributary of the Nile ( $\delta_{V20} = +0.94$ ,  $\sigma_{V15} = 0.14$  and  $\sigma_{V20} = 0.29$ ). The updated V20 fields increased the lake fraction reducing from 0.36 in V15 to zero in V20. The lake depth has been similarly decreased from 25m to 6m. However, whilst this is a very dry region, this grid cell also contains a section of the Toshka Lakes (Fig ??), a collection of endoheic lakes, newly formed (and growing) due to overflow from Lake Nasser. These lakes are known to be highly time variable, with a periodic seasonality on top of the general increasing lake sizes, and the formation of surrounding wetlands. These lakes rapidly fill and dry out; at this point from 0 to 0.14. The grid cell contains the Upper Atbara and Setit Dam Complex. However, the dam was only recently completed in 2018 – during the training and validation years – along with the decade before the lakes were mostly dry (Tos), whereas during the testing year they were filled. Whilst these are the major regions where the period the dam was still under construction. Consequently whilst the V20 prediction is significantly worse than the field may be more accurate at the current time, during the period the model was training the V15 prediction, there are other regions of note where the underperformance is less severe. For example in parts of northern Canada there is a notable population of red points, where for the Northwest Territories the mean  $\delta_{V20}$  is +0.02K. This difference is slight and it is hard to draw any definitive conclusions – whilst some grid points get better, some get worse. For these high latitude regions there is a large variability over the course of the year as field was more accurate, since the dam was not yet built.

– **Lake Tuz**. This grid cell contains a large fraction of Lake Tuz as well as the smaller Lake Tersakan, saline lakes in central Turkey ( $\delta_{V20} = +0.85$ ,  $\sigma_{V15} = 0.25$  and  $\sigma_{V20} = 0.34$ ). Here the updated physiographic field effectively removed all lake water, with the water freezes in the cold season and then melts during the summer. Such a time variability is not ideally captured by lake parametrisation which is likely the cause of the issues here, along with the greater uncertainty and error

in the observations in these regions with increased cloud cover. Another interesting location is the north eastern edge of the Caspian Sea, where there are 4 grid points with a mean  $\delta_{V20} = +0.65$ K. This is the Astrakhan Nature Reserve, an extensive wetlands region. In going from V15 to V20, the lake fractions have generally been decreased and the vegetation fractions increased correspondingly lake fraction decreasing from 0.14 to 0.005. Whilst the lake is shallow and does dry out in the summer, there is also a large fraction of surface water present (e.g. Fig 10d) and it is an over correction to completely remove all lake water at this point.

– **Lake Urmia**. This grid cell contains Lake Urmia, which is another saline lake in Iran ( $\delta_{V20} = +0.81$ ,  $\sigma_{V15} = 0.12$  and  $\sigma_{V20} = 0.73$ ). The updated physiographic fields decreased the lake fraction at this point from 0.77 to 0.39. This was in response to the shrinking of Lake Urmia due to long-timescale droughts and the damming of rivers in Iran. However, since these are wetlands there is likely a large degree of water present and the updated V20 lake fields may be insufficiency informative and an extra map of wetlands may be necessary. This drought broke in 2019 and Lake Urmia is now increasing in size again – satellite imagery now shows a large fraction of the grid cell covered by water (Figure 10f).

We can also inspect the subclass of the Lake Updates category, The Lake-Ground Updates, and restrict our sub-category, which restricts analysis to only points where there was with no significant change in the vegetation. This then allows us to more clearly see the effect of adding/removing water without the additional influence due to the change in vegetation. In this case the mean improvement in the prediction accuracy when using the on/from bare ground. This sub-category shows even larger improvements in LST predictability if using V20 fields is stronger than the Lake category, with  $\delta_{V20} = -1.12$ K field set instead of V15 (see Table 4) – prediction accuracy increased globally (over 546 grid-cells) on average by 0.83K ( $\sigma_{V15} = 0.15$  and  $\sigma_{V20} = 0.04$ , see also Figure 7). This indicates that whilst the updated lake fields are globally accurate and informative, providing on average over the globe, over a year, more than nearly an extra Kelvin of predictive performance, the updates to the vegetation fields tamper this performance gain. This suggests at a, indicating potential problem with the vegetation fields , which we will now explore further.

### 3.1.2 Category: Vegetation Updates

Whilst the edits to the V15 lake fields generally act to increase the prediction accuracy, indicating that these fields are accurate and informative, changes to the vegetation generally give worse predictions. We can see from Table

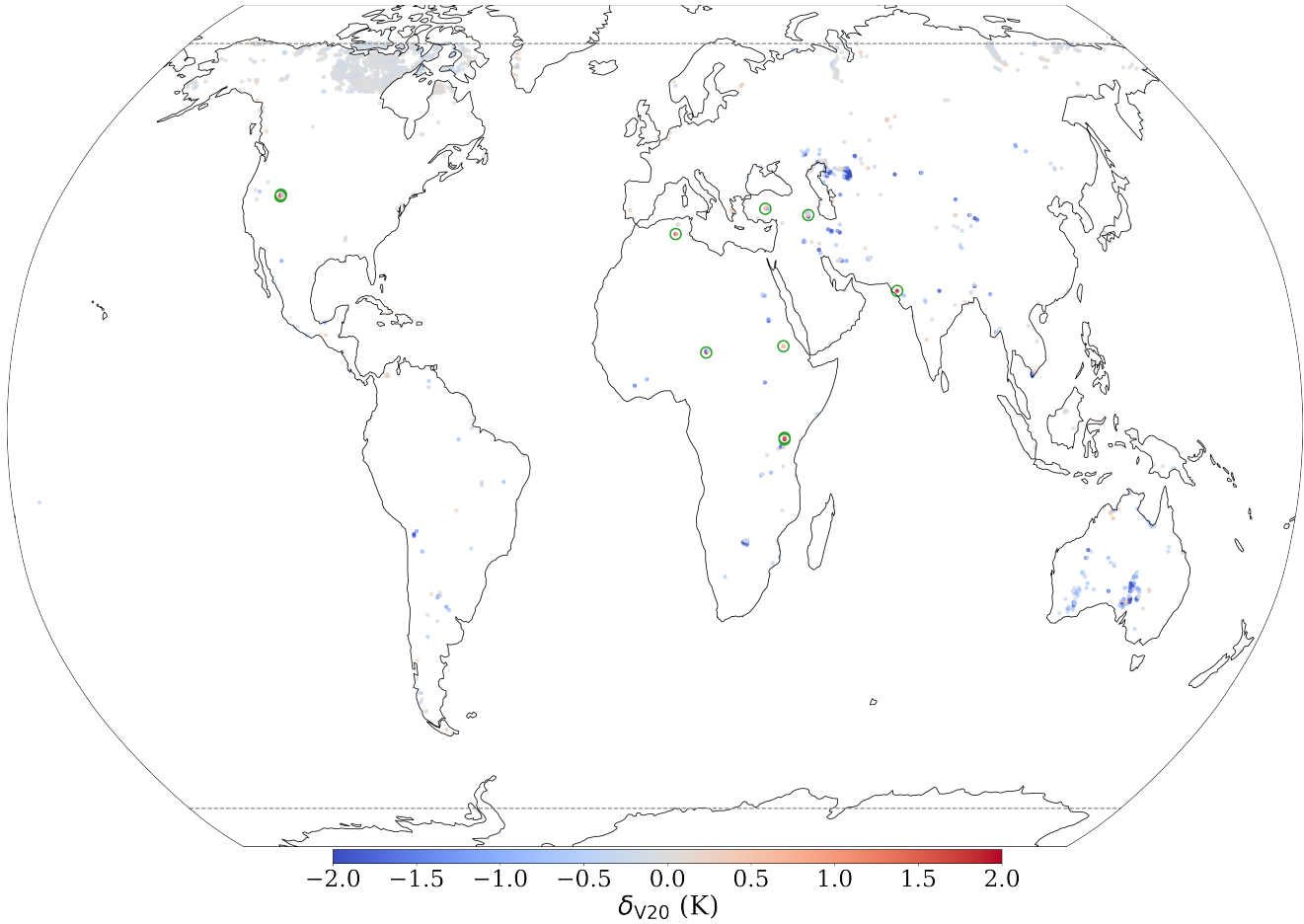


**Figure 9.** Differences in the prediction error MAE, between VESPER V20 and VESPER V15, (i.e.  $\delta_{V20}$ ) for 2019 at 31km resolution for ‘Lake Updates’ category (i.e. where lake cover changed significantly). Generally, VESPER V20 LST predictions are more accurate, for example in the Aral sea and Australia, indicating that V20 field set is informative and accurate. Particular points where VESPER V20 LST prediction gets notably worse compared to VESPER V15 are highlighted with green circles and discussed in the text.

?? that the mean prediction accuracy when using the updated fields decreases by 0.49K over 58 points. For all points apart from one, the *cvh* The Vegetation updates category, restricts analysis to grid points with significant change to high vegetation cover, where the high vegetation cover is substituted with either low vegetation or bare ground, and vice versa. For this category the prediction accuracy of V20 decreased globally (over 58 grid-cells only) on average by 0.04K. However, this shift is much smaller than the training noise between successive VESPER iterations ( $\sigma_{V15} = 0.04$ ,  $\sigma_{V20} = 0.15$ ) and so it is hard to make definitive statements about the performance of the updated vegetation physiographic fields as a whole (see e.g. Fig 13). The best we can say is that the updated V20 vegetation fields offer no global improvement in the LST prediction accuracy.

If we isolate our analysis to individual grid points where the training noise is small (highlighted by \* points in Fig 13) we can discern that there are multiple locations where the

high vegetation fraction was decreased, (often quite drastically to zero, i.e.), specifying that there should just be bare ground in these grid boxes. Whilst this may be accurate for some points, by inspecting, but thorough inspection of these areas with satellite imagery it is clear that there are regions which are in fact areas of revealed that they should in fact be covered with high vegetation (see e.g. Fig 12) and that it is inaccurate to simply remove all vegetation from these grid boxes. It is also notable that the grid points which have the largest drop in predictive performance when going from V15 to updating the V20 are all grid points where the vegetation fraction is severely high vegetation cover was erroneous for these grid-cells. Moreover, for this subset of less noisy grid points, the strength of the drop in LST predictability in VESPER V20 comparing to VESPER V15 is approximately linearly dependent to the degree of reduction in high vegetation fraction, when the vegetation is replaced with bare ground (i.e.  $\delta_{V20}$  is maximally positive when the grid-cell that was fully covered

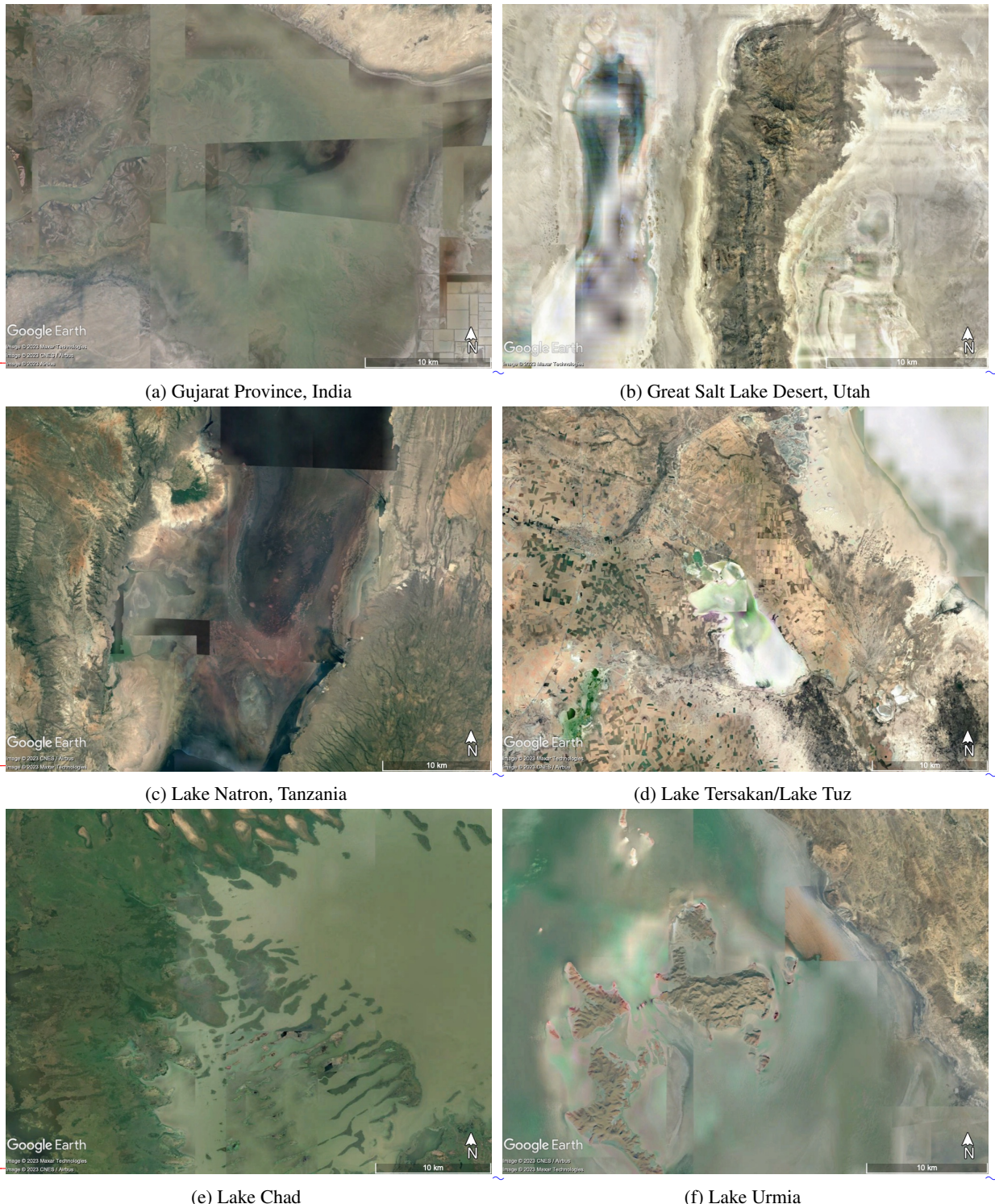


**Figure 10.** Satellite A selection of satellite imagery of some of the problematic Lake Updates points highlighted in Fig. 9 where the V20 predictions are worse than the V15 predictions. Generally the updated V20 fields remove water, only considering permanent water. However these regions have highly time variable waters, which are better captured on average by the V15 fields. The images are centred on the grid box coordinates. **Note that the lengthscales are different for some images.**

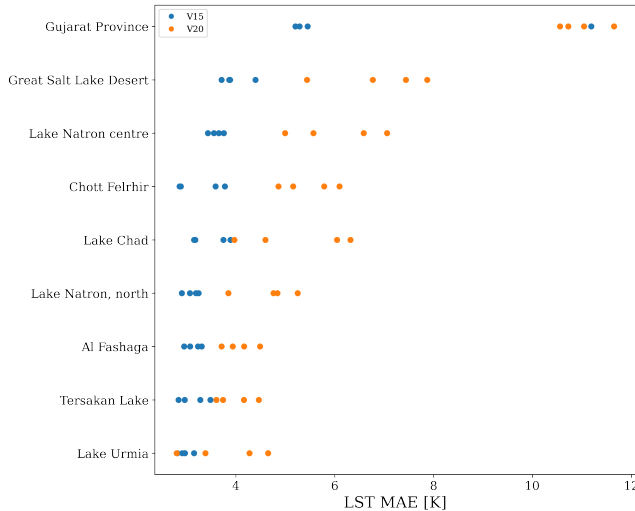


**Figure 11.** As Fig. 7 for selected locations in the lakes grid point category where the added V20 data results in worse predictions when compared to V15.

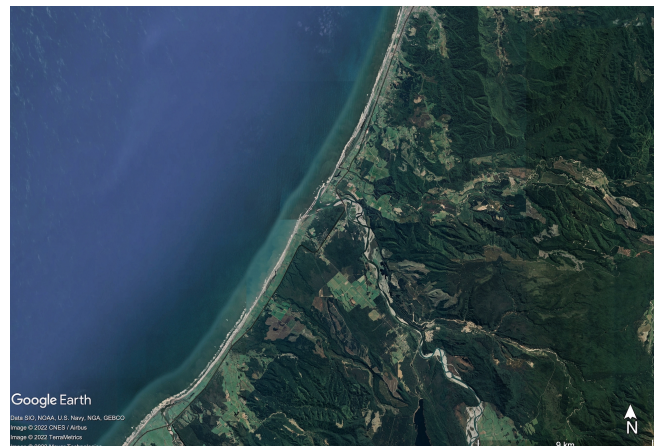
with forest becomes fully covered with bare ground – high vegetation cover is reduced to zero. This suggests that such extreme changes may be strong over-corrections, and more modest updates to the vegetation fields may be more accurate. These erroneous ( ). These erroneous grid-cells in V20 vegetation fields are likely inherited from initial datasets used to update vegetation or to appear during the interpolation. The errors in these regions will in turn corrupt the LST predictions and mitigate the gain from a more accurate representation of the lake water. The majority of grid cells in this category (57/58) are modified in this way where the high vegetation fraction is severely reduced, however due to the large degree of training noise and the small number of points, it is difficult to draw any definitive conclusions for the category as a whole.

### 3.1.3 Category: Glacier Updates

The Glacier Updates category in general shows improvement in LST predictability in VESPER. V20 updates to the glacier fraction also generally improve the predictions, with a mean  $\delta_{V20} = -0.14$  K comparing to VESPER V15 (see Table 4) – prediction accuracy increases globally (over 1057 grid points. These improvements are concentrated grid-cells) on average by 0.22K ( $\sigma_{V15} = 0.03$ ,  $\sigma_{V20} = 0.02$ , most notably) around the Himalayas, the land either side of the Davis strait, as well as British Columbia and the Alaskan Gulf. Analogous to the Lakes Updates category whilst the introduction of the V20 fields generally improves the model, there are some selected regions glacier cover generally improves LST predictions, there is a small selection of grid points where the prediction gets worse. These are heavily concentrated in the southern hemisphere, in particular



(a)



(b)

**Figure 12.** Satellite imagery of grid-boxes grid-cells in (a) (a) Siberut Island, Indonesia and (b) (b) South Island, New Zealand. For both points it is expected grid-cells according to the updated V20 fields that field set there is should be no vegetation, just bare ground. VESPER can identify identified these erroneous updated fields areas.

on the south-western edge of South America and the South Shetland Islands (which lie closer to Antarctica as well as), and some parts of the Himalayas. This deficit deterioration in performance in these areas is not due to erroneous updated update of V20 fields, but instead is a data quality issue whereby we do not have a lot of MODIS observations in these areas which have a large degree of orography and cloud cover. This can be seen in Fig ?? for the above mentioned regions. Consequently the neural net model glacier cover, but related to the Aqua-MODIS data (i.e. sparse availability due to clouds, and less certain due to orography, see Figure 5a). Consequently, VESPER finds it difficult to make accurate predictions in this region, and this iteration of the model has settled into a local minimum for V20 which is worse than and for these

35

40

45

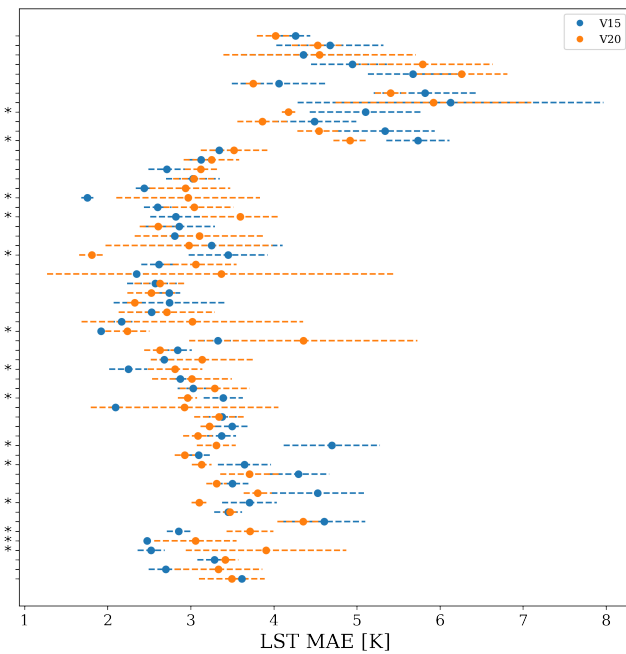


**Figure 13.** Distribution of prediction errors in the LST, for VESPER V15 and VESPER V20, for all 58 grid points in the vegetation category. There is evidently a large degree of noise, with predictions from both generations of VESPER model highly overlapping. Points with reduced training noise are highlighted with a \*.

points there is often a large degree of training noise, with considerable overlap between VESPER V15 in these areas. If we isolate just grid points where we have a large number of observations (we take and VESPER V20. If grid- cells with scarce amount of Aqua-MODIS observations (i.e. mean number of MODIS observations per ERA data point  $> 50$ ) Aqua-MODIS observations per day over the year per ERA5 grid-cell is  $> 50$ ) are removed from the analysis then the worst performing grid points are excluded. In this case 5 there do remain grid-cells become excluded, yet a few areas where the VESPER V20 model underperforms with respect to underperforms VESPER V15 remain. For example, there is a grid point in the Alaskan gulf on the Bering Glacier with  $\delta_{V20} = +2.16$  K. This point grid-cell in 10 Chilean Patagonia that contains the Calluqueo Glacier, close to Monte San Lorenzo where  $\delta_{V20} = 2.49$  ( $\sigma_{V15} = 0.38$ ,  $\sigma_{V20} = 0.62$ ). This grid-cell has been updated in V20 to 15 have a higher glacier proportion (0.68 to 0.92), such that the grid box should be almost completely dominated by ice. Nearly all low-vegetation was also completely removed (cvl from 0.10 to 0.007) and the lake depth increased from  $\sim 2$  m to  $\sim 27$ , in conjunction with a modest decrease in the lake fraction, from 0.07 to 0.01. Satellite imagery of the 20 region (Fig. 14) shows an area that does have a significant ice fraction, but perhaps not as great as  $\gtrsim 90\%$ , suggesting 25

that the V20 updates field set comparing to V15 by strongly increasing glacier cover from 0.0 to 0.44), decreasing low vegetation cover (from 0.22 to 0.12) and high vegetation cover (from 0.16 to 0.09) as well as modestly decreasing lake cover (from 0.02 to 0.007). According to satellite imagery (see Figure 14a) the glacier only occupies a small fraction of the overall grid-cell, and the updated glacier cover may have been an over correction. The Bering glacier is also known to be a time variable region which varies in size over the course of the season, whilst on longer timescales exhibits a general retreat of the terminus over time, coupled with periodic surges in the glacier flow around every 20 years Molnia and Post (2010). It is therefore a complex region not necessarily well represented by a static fractional field. There also appears to be some low-level vegetation present, and again removing all vegetation for this region may have been an overcorrection. Another notable grid Moreover, this is an complex orographic area with snowy mountain peaks at high altitude and deep valleys, therefore the temperature response due to the glacier feature could be atypical compared to e.g. the Alaskan Gulf or the Davis straight. There is also substantial vegetation cover in the valleys that may not be being properly described. A similar point is in the Chilean Andes (see Figure 14b), by the Juncal Glacier. Here the ice fraction was increased in with  $\delta_{V20} = 1.26$  ( $\sigma_{V15} = 0.68$ ,  $\sigma_{V20} = 0.29$ ). Here V20 glacier cover was increased to 0.25 from zero compared to 0.00 in V15, an attempt to better represent the glacial ice. However,  $\delta_{V20} = +2.67$  K. In fact, the glacier itself only occupies . Again, this is may have been an over correction, as the glacier constitutes only a small fraction of the overall grid box, and the updated field may have been an over correction. Moreover, this is grid cell. As with the Calluqueo Glacier this is also an area with lots of orography , with snowy mountains at high altitude and deep valleys. Therefore the temperature response due to the glacier feature could be atypical compared to e. g. the Alaskan Gulf or the Davis straight. For both these points we can again see how VESPER 's ability to identify grid points where the model predictions become worse in this way is a powerful tool for identifying updated fields or regions which are insufficiently accurate or informative, and so could have an atypical temperature response. For both of these points VESPER managed to identify potential inaccuracies in updated glacier cover, and once again proved itself as a useful tool for quality control of surface physiographic fields.

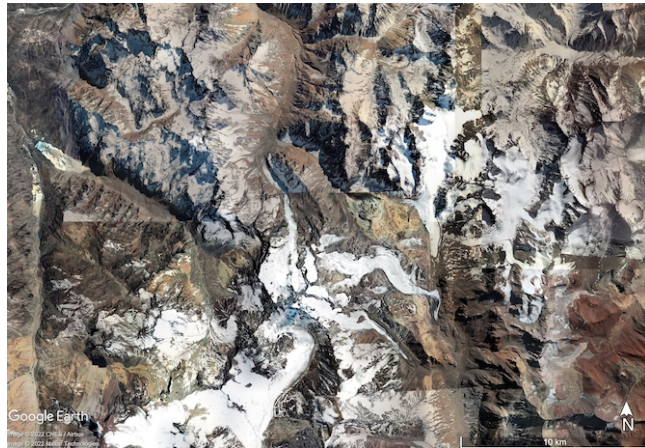
From this example deploying VESPER on the lake parametrisation fields,

### 3.2 Evaluation of new lake fields: Monthly water & salt lakes

From the examples above it is evident that VESPER enables the user to quickly identify regions where the new parametrisation works effectively update to surface



(a)



(b)

**Figure 14.** Satellite imagery of (a) Bering (a) Calluqueo Glacier, Alaskan Gulf Patagonia, and (b) (b) Juncal Glacier, Chile. For (a) it is expected that there is no vegetation and In the grid box to be primarily ( $\gtrsim 90\%$ ) dominated by ice. For (b) the updated V20 fields specify a  $\gtrsim 25\%$  glacier fraction. Evidently field set, the V20 fields assumption for region (a) is almost half ice cover with little vegetation, for region (b) is quarter covered with glacier; these grid boxes are assumptions seem to be insufficiently accurate or informative, as identified by VESPER.

help of VESPER.

15

### 3.3 V20X: Monthly water & salt lakes

Particular regions where it was difficult for the model to make predictions—VESPER was struggling to make accurate LST predictions—especially with the updated V20 fields field set which only include permanent water—were either areas with a large degree of temporal variability (e.g. lakes which flood and dry out periodically, or freeze and melt) or else lakes which are salt water rather than fresh water areas with saline rather than freshwater lakes. Clearly if the size, shape and depth of a lake are changing over the course of the year, these are going to be hugely significant factors in modelling the lake temperature response. Similarly, saline lakes behave very differently to fresh water freshwater lakes since increased salt concentrations affect the density, specific heat capacity, thermal conductivity, and turbidity, as well as evaporation rates, ice formation and ultimately the surface temperature. These two properties of time variability and salinity are often related; it is common for saline lakes to flood and dry out over the course of the season, which naturally also affects the relative saline concentration of the lake itself.

20

25

30

35

40

45

50

55

60

65

Currently, neither the VESPER V15 or VESPER V20 models have any information regarding the salinity of the lakes or their time variability. Indeed, FLake is specifically a fresh water lake model! We can introduce this information by also This information can be introduced by including a global salt lake map and monthly inland water lake map as saline lake cover and monthly varying lake cover as additional VESPER's input features, and use VESPER to investigate the added value of these additional fields. To create a monthly inland water map we first create 12 monthly fractional land sea masks based on JRC Monthly Water History v1.3 maps for 2010–2020. Since the annual lake maps were created taking into account a lot of additional sources we enforce the extra condition on the monthly maps that the monthly water is equal or greater than permanent water distribution from fractional land sea mask. To create an inland salt water map we used the salt lake list from GLDBv3. First, in order to identify separate lakes on inland water map, we mask small sub-grid lakes and large lake coasts, i.e. grid cells that have water fraction less than 0.25. Next, we compute number of connected grid cells in each lake (i.e. connected with sides only). Then we vectorise only lakes that have 100 and more connected grid cells, as at ERA5 resolution of  $\sim 31$  km the grid cells are quite large and can include a mixture of freshwater and saline lakes. Finally, saline lake vectors are selected by filtering vectors which have no saline lake point located from GLDBv3. This process resulted in a map at 31 km resolution based on 147 large salt lake vectors. In the

physiographic fields was beneficial (e.g. Aral Sea) as well as spotting regions where it is less performant and where it was not (e.g. Lake Natron, high vegetation updates). In turn, those areas where the areas where LST predictions do not improve as expected can be inspected and erroneous or sub-optimal representations of the surface physiographic fields identified. This then provides key information on how to introduce further and where to introduce additional corrections to better represent these more difficult challenging or complex regions. We will now further explore some Some of these problematic areas and demonstrate how VESPER can guide the development and introduction of additional surface fields are now explored in more details and additional surface physiographic fields introduced with

future we plan to revisit the map of salt lakes and extend the list to include additional data.

We create a new model iteration “then using VESPER to rapidly assess the accuracy of these new surface physiography fields and evaluate if their use in the model increase LST predictability. We define an additional models (see Table 3 for a summary of all VESPER models used in this work); VESPER\_V20X “which is analogous to the uses the same field set is the same as VESPER\_V20 model, but now also has as input features the monthly water (a quasi-time variable field) and the salt lake cover (a static field). We again train the model on 2016 and make predictions for 2019. The results are presented alongside the but with additional saline lake cover and monthly-varying lake cover. The results of this model in comparison with VESPER\_V15 and VESPER\_V20 results in Table 22. is summarised in Tables 4, 5. We will now explore the influence of the additional saline maps and monthly lake maps in more detail.

### 3.2.1 Category: Lake Updates

We can see that for the The Lake Updates category , the prediction accuracy averaged over the year is effectively unchanged from the shows no significant difference in LST predictability globally when using the V20X field set instead of V20model. with  $\delta_{V20X} = \delta_{V20} = -0.37$  (comparable training noise). For the Lake-Ground-Updates category, the accuracy has decreased slightly, from  $\delta_{V20} = -1.12$  K to  $\delta_{V20X} = -1.09$  K, although the difference is so small as to be within the model noise. The equivalence of the annually averaged V20X and Lake-ground category, there is a modest increase, with  $\delta_{V20X} = -0.84$  compared to  $\delta_{V20} = -0.83$  but this is within the training noise.

For Lake Blanche, V20X reduces the prediction error by 2.43K compared to some of the problematic lake grid-cells highlighted in Table 5, the addition of saline maps and monthly lake maps does improve the LST predictability relative to VESPER\_V20. This is in spite of the fact that our salt lake maps do not identify Lake Blanche as a salt lake, and so all the improvement in the prediction is from the additional information from the monthly lake maps. The salt lake maps are similarly inaccurate for the grid point in Northern India, failing to recognise the underlying salt marsh. However, again the information contained in the monthly lake maps allows the reduction in the error by 2.19K. There are also regions where the saline maps are correct to not specify any salinity, such as in Afghanistan and the Toshka lakes; again the monthly maps provided sufficient information to allow for a marked improvement by 2.04 K and 2.15 K respectively. This is particularly notable since the size of the monthly lake corrections is small for these points: the mean monthly correction for Afghanistan is 0.046 and for the Toshka Lakes is 0.001. However, under the updated V20 both of these areas have had all water

removed and so adding in just a small amount of time variable water allows for much more accurate predictions.

This example illustrates how VESPER both can identify inaccurate fields and quantify the value of updated fields, as well as emphasizing the importance of time variable lake fields more generally. For points where the saline maps do

specify that the underlying lakes are salt lakes – Lake Natron and . For the Great Salt Lake Desert it is not possible to disentangle whether the gain is due to the saline maps or the monthly maps. The centre of Lake Natron exhibits a particularly notable improvement by 2.6K, whilst for the grid point on the northern edge the gain is more modest at 0.12K.

This is likely due to the fact that the updated monthly maps provided much stronger corrections at the centre of the lake (mean correction 0.13) than at the northern edge (mean correction 0.02). For , Chott Fehrir, Lake Chad and Lake Urmia, VESPER\_V20X is a notable improvement over VESPER\_V20 with  $\delta_{V20X} = 0.248, 0.726, 0.029, 0.22$  respectively. The difference in  $\delta_{V20X}$  and  $\delta_{V20}$  for these points is greater than the training noise. If we take as a case example the grid point at in the Great Salt Lake

Desert, the improvement is 2.06 K again with in using VESPER\_V20X over VESPER\_V20 is  $2.667 \text{ K} \pm 1.10 \text{ K}$ . At this point there is a strong correction from the monthly lake maps (mean value 0.16) and the salt maps (mean value 0.56). This improvement is to be expected given the known strong salinity and time variability in the region, and so it

is a nice confirmation to have these updated fields verified by VESPER. It is also notable that the variation in the monthly lake maps at this point is very large, with a standard deviation in the lake fraction over 12 months of 0.18. At the start of the year the corrections from the monthly maps are

very large, then as the year progresses the magnitude of the corrections generally decreases as the lake dries out. Such a large variation is again difficult to ever capture with a static field.

Other regions of note that we have mentioned previously are the Northwest Territories and the Nunavut province in Northern Canada where the It is however notable that

a) for all of the problematic lake points that we have discussed  $\delta_{V20X}$  is positive and b) there are multiple points (e.g. Gujarat province) where VESPER\_20X exhibits no improvement over VESPER\_V20 model underperformed

relative to V15, with  $\delta_{V20} = +0.02$  K. The introduction of the monthly lake maps modestly improves the predictions in this area, with  $\delta_{V20X} = -0.03$  K. In these high-latitude

regions one might expect some time variability due to freezing and thawing of the lake surfaces, and the addition of the monthly lake maps to the model then provides some of this time variable information, allowing for improved predictions. Whilst this is an improvement, the effect is modest; it is generally difficult to get quality observations at high latitudes, especially during the cold season, due to increased cloud cover. Therefore whilst VESPER can say

Category	Grid-cells/location	$\sigma_{VM}, K$				$\delta_{VM}, K$		
		V15	V15X	V20	V20X	V15X	V20	V20X
Lake	Gujarat Province, India	2.54	1.12	0.42	1.04	-1.26	4.21	5.24
	Great Salt Lake Desert, Utah	0.26	0.41	0.92	0.62	-0.18	2.92	0.25
	Lake Natron centre, Tanzania	0.12	1.48	0.81	0.53	1.35	2.45	2.61
	Lake Natron north, Tanzania	0.13	0.37	0.51	0.18	0.72	1.57	1.24
	Chott Felhrir	0.41	0.57	0.49	0.58	0.34	2.20	0.73
	Lake Chad	0.33	1.21	0.98	0.96	0.29	1.74	0.03
	Al Fashaga	0.14	0.08	0.29	0.42	-0.24	0.94	1.06
	Tersakan Lake	0.25	0.20	0.34	0.38	-0.00	0.85	0.99
Glacier	Lake Urmia	0.12	0.54	0.73	0.32	0.54	0.82	0.22
	Callqueo Glacier, Patagonia	0.38	0.62	1.60	0.73	0.08	2.49	0.32
	Juncal Glacier, Chilean Andes	0.68	0.29	1.06	0.36	0.11	1.26	1.20

**Table 5.** As Table 4 for specific grid points discussed in the text where the VESPER\_V20 predictions are worse than VESPER\_V15 (i.e.  $\delta_{V20}$  is positive).

that the addition of the monthly lake maps does improves the predictions in these regions, for improved performance cloud-independent data should be used. Additionally, the corrections from the monthly lake maps are small in these regions, with a mean correction of 0.02 and a generally small variance; in actuality time-variable fields with greater variance over the year may be more accurate. Due to the freezing and thawing, improving ice on/off date prediction by the lake parametrisation should help better describe the seasonality and variance.

It is worth emphasising that whilst the V20 and V20X models are improvements over V15 globally, and V20X is generally an improvement over V20 for these problematic points, there are regions where neither V20 or V20X outperform V15 ( $\delta_M$  is always positive), such as Lake Natron and Northern India within training noise. Given all the extra information provided to the more advanced models VESPER\_20X model this is unusual, unless; it suggests that either i) some of the additional information is erroneous in these regions or else, or else ii) the temperature response is completely atypical to the rest of the globe and. For point ii), this means that the additional information is not predictive in these regions. To explore this hypotheses we Including this additional information in our neural network increases the complexity of the model which may in turn increase its training noise. This is likely the reason behind point b) - the updated fields are not sufficiently informative but do increase the training noise and so we see no improvement from using VESPER\_V20X. For example, for Gujarat province  $\sigma_{V20} = 0.416$ , but  $\sigma_{V20X} = 1.04$ . In order to explore the hypothesis of point i) we train one further model, VESPER\_V15X. This (again, see Table 3 for a summary of all VESPER models used in this work). This VESPER iteration is analogous to VESPER\_V20X, being simply the VESPER\_V15 model with the additional monthly maps and salt lake fields included. Importantly it does not have the updated physiographic correction fields from V20.

Globally, this model performs worse than the V20 models, as we might expect - for example in the Lake Updates category  $\delta_{V15X} = -0.25\text{K}$  compared to  $\delta_{20X} = -0.45\text{K}$ ,  $\delta_{V15X} = -0.20$  ( $\sigma_{V15X} = 0.02$ ) compared to  $\delta_{V20} = -0.37\text{K}$ . However, VESPER\_V15X does perform well at these problematic a number of the these problematic lake points (see Table 225). For both the Lake Natron grid points V15 outperforms 7 out of the 9 selected lake points, VESPER\_V15X outperforms VESPER\_V20X, suggesting that at this location. For example in Gujarat province the improvement in using V15X over V20X is  $6.5\text{K} \pm 1.53$ . This suggests that our hypothesis for point i) is correct and that for some grid points the V20 fields are generally less accurate than the V15 fields. For a subset of points VESPER\_V15X however underperforms relative to also outperforms VESPER\_V15 which also indicates that the monthly maps and the salt lakes are either inaccurate at this location, or that the temperature response of Lake Natron is highly atypical. For Northern India, the performance of the V15 model is particularly striking, whilst the V20 and V20X models struggled to make more accurate predictions than V15, V15X decreases the average prediction error by nearly 6K. This again indicates that for this point the V20 fields are less accurate than V15. Similarly for the Great Salt Lake Desert,  $\delta_{V20} = 1.78\text{K}$ ,  $\delta_{V20X} = -0.28\text{K}$  but  $\delta_{V15X} = -0.86\text{K}$ , which suggests that whilst the monthly lake maps and the salt lake fractions are accurate and informative in this area, the static V20 fields are not (e.g. for Gujarat province  $\delta_{V15X} = -1.26$ ) but the difference is typically within or close to the training noise (e.g. for Gujarat  $\sigma_{V15X} = 1.12$ ) and so it is hard to draw any strong conclusions. These examples illustrates again how VESPER can identify particular regions where the fields are inaccurate, as well as emphasising the need more generally for accurate descriptions of seasonally varying inland water and saline lake maps in Earth system modelling.

### 3.2.2 Category: Vegetation Updates

Whilst the Vegetation Updates category explicitly deals with areas where the lake fraction does not change when going from V15 to V20, many of the grid points in this category do contain some kind of waterbody, often lying close to the coast or else containing lakes or large rivers. Information on the salinity and temporal variability of these water bodies ~~can~~ ~~could~~ then influence the prediction accuracy. By providing the additional information in ~~V20X~~, the mean  $\delta_M$  is reduced from  $\delta_{V20} = +0.049\text{K}$  to  $\delta_{V20X} = 0.005\text{K}$ . This performance is gained despite the known errors for some of the grid boxes in the *cvh* vegetation updates (e.g. Figure 12), again demonstrating the importance of salinity and seasonally varying water. The ~~V15X~~ model is less performant than ~~V20X~~, with  $\delta_{V15X} = 0.11\text{K}$  since there ~~are~~ some grid boxes in this category where the updated ~~V20~~ fields are accurate and valuable if augmented by monthly variability. However if we consider just the worst performing grid points where  $\delta_{V20} > 1\text{ K}$  then the mean values are  $\delta_{V20} = 2.0\text{ K}$ ,  $\delta_{V20X} = 0.49\text{ K}$  and  $\delta_{V15X} = 0.21\text{ K}$ . This again demonstrates how the *cvh* fields have been erroneously updated for a small selection of grid points in ~~V20~~. ~~VESPER~~ ~~V20X~~, the error relative to ~~VESPER~~ ~~V15~~ is reduced modestly to  $-3 \times 10^{-4}$  although as we saw before with the vegetation category the noise is large  $\sigma_{V20X} = 0.21$  and so it is difficult to draw any further definitive conclusions. Similar arguments apply to ~~VESPER~~ ~~V15X~~.

### 3.2.3 Category: Glacier Updates

We would expect the additional information provided by the ~~V20X~~ fields to be particularly effective for glacial grid points. Glacier ice is naturally found next to waterbodies which freeze and thaw over the year, and the salinity of water will also influence this freezing. Therefore accurate additional information from the monthly lake maps and the saline maps should prove useful in these more time variable regions. This is indeed what we observe with the mean delta going from  $\delta_{V20} = -0.13\text{K}$  to  $\delta_{V20X} = -0.24\text{K}$ . Considering the two problematic points that we discussed previously, in the Alaskan Gulf the prediction accuracy relative to ~~V15~~ has improved from  $\delta_{V20} = +2.16\text{ K}$  to  $\delta_{V20X} = +1.00\text{ K}$ , whilst for the Juncal Glacier We do observe a small improvement globally, with  $\delta_{V20X} = -0.28$  compared to  $\delta_{V20} = -0.22$ , however this difference is comparable to the prediction accuracy has also improved, with  $\delta_{V20X}$  decreasing to  $+1.88\text{ K}$ . Despite this improvement, again for both of these points the prediction accuracy still lags behind ~~V15~~. This is on account of the training noise  $\sigma_{V20X} = 0.06$ . This training noise could be slightly deceptive; 3 out of our 4 ~~VESPER~~ ~~V20X~~ iterations outperform every ~~VESPER~~ ~~V20~~ fields being insufficiently accurate in these areas, as has been discussed. Neither

of these grid points correspond to saline lakes or have a significant time variability in iteration in the Glacier Updates category. The 4th ~~VESPER~~ ~~V20X~~ iteration is somewhat anomalous - the increased network complexity could mean that the model did not converge well for that particular iteration, for the ~~monthly~~ lake fractions and so are also not improved by a glacier grid points. Since the updated ~~V20~~ glacier fields are generally accurate globally, we saw no particular improvement in using ~~VESPER~~ ~~V15X~~ model to within the training noise. This suggests that the additional monthly lake maps are only useful if the underlying representation of static water is sufficiently accurate. Considering the particular glacier grid points we discussed previously in Section 3.1.3, the additional monthly lake maps were particularly useful for the Callqueo glacier, with  $\delta_{V20X} = 0.32$  compared to  $\delta_{V20} = 2.49$  ( $\sigma_{V20} = 1.59$ ,  $\sigma_{V20X} = 0.73$ ). However we saw no improvement to within the training noise for the Juncal glacier.

### 3.2.4 Timeseries

Thus far we have been focusing mainly on the  $\delta_M$   $\delta_M$  metric averaged over the entire year of the test set. It is also of interest to explore how the prediction error for each of the 3 models varies with time. This is demonstrated in Fig 15 for each of the 4 updated categories that we have discussed.

For the Lake Updates and Lake-Ground Updates categories we can see that all the model predictions track the same general profile, with the error peaking in the northern hemisphere summer months. This is a result of FLake modelling being least accurate during the summer as the lake is not fully mixed and so the mixed layer depth for lakes is too shallow, resulting in skin temperatures with larger errors. Conversely, in the autumn and spring the lake is fully mixed and predictions have the smallest errors compared with observations. A clear hierarchy of models is evident; the ~~VESPER~~ ~~V15~~ and ~~VESPER~~ ~~V20~~ ~~V20X~~ models consistently outperform the ~~VESPER~~ ~~V15~~ model across the year. This again is solid strong evidence, highlighted by ~~VESPER~~, of the value of the updated fields both static and seasonally varying. We mentioned discussed previously how the annually and globally averaged  $\delta_M$   $\delta_M$  values for the Lake Updates category were highly comparable for ~~VESPER~~ ~~V20~~ and ~~VESPER~~ ~~V20X~~, despite ~~V20X~~ significantly improving the worst behaving points. We can see from the top panel in Figure 15 that the this equivalence is not consistent over the year. Instead, during the winter months of the northern hemisphere ~~VESPER~~ ~~V20~~ and ~~VESPER~~ ~~V20X~~ model is a systematic improvement on are fairly equivalent; ~~VESPER~~ ~~V20~~ from around April onwards, but at earlier times in the year ~~V20~~ outperforms tends to outperform ~~VESPER~~ ~~V20X~~, but the difference is within the model training noise. However in the central months of the year ~~VESPER~~ ~~V20X~~ starts to be slightly

more accurate. This is likely for two reasons. Firstly, the monthly lake maps are in fact a climatology and therefore insufficiently precise to detect the exact ice on/off dates during the winter months, where we have a large number of 5 grid points at high latitudes which will be subject to freezing, nullifying any time variability. Secondly, The second reason is due to the accuracy of the lake mean depth which strongly drives the ice on-dates due to its influence on the heat capacity of the lake. During the warmer months lakes thaw, 10 the monthly maps are more accurate, as the thawing of lake ice is mainly connected to the atmospheric conditions, not the lake depth, and so the information contained in them can be used to make more accurate predictions.

15 The Lake-Ground Updates timeseries broadly follows the same general profile as Lake Updates, but the errors are larger - those grid points where the lakes have been replaced with bare ground were particularly poorly described in V15. Additionally, for Lake Updates we see two sharp decreases in 20 the prediction error during  $\sim$  April and September, which are not as strongly reflected in Lake-Ground. This is due to the geographic location of the grid points in each of the two categories; for the Lake Updates category the grid points are located primarily in the boreal zones and so are subject to 25 freezing and thawing over the course of the year leading to a strong seasonality due to the lake mixing that we have discussed. The sharp drop in April corresponds to a time where the lakes are unfrozen and fully mixed. However the lakes in the Lake-Ground sub-category are less concentrated and 30 much more evenly distributed over the globe and so do not exhibit such a strong seasonality.

Examining the timeseries for Vegetation Updates, whilst there is a large degree of variability, we again see the trend 35 previously discussed whereby the V20 fields make the predictions systematically worse across the entirety of the test year. The introduction of the monthly lake maps in V20X compensates for the erroneous V20 vegetation fields - the V20X predictions are generally worse than V15 at the start and end of the year, but better in the middle. This 40 is due to the fact that the majority of Consistent with our previous discussion, the points in the Vegetation Updates category are in climate zones which have pronounced rainy and dry seasons e.g. Indonesia, the Amazon. At the start 45 training noise makes it difficult to separate the predictions of the VESPER model for the vegetation category across the year during. All generations of VESPER VM follow the same general trend, with errors maximal at the start and end of the wet season there is lots of precipitation and the static V15 fields are generally more accurate. As the 50 rains abate and the dry season starts the V15 lake fields are underestimates which are then improved through the introduction of additional water via the monthly lake maps. year, and minimal during the spring and autumn months.

For Glacier updates we can For the Glacier updates category, in order to deal with the separate warming and cooling seasonal cycles over the year, we separate grid points into the northern and southern hemispheres. We again consider just those points where the number of MODIS observations at a given instant in time, per ERA data point is greater than 50. For the northern hemisphere the familiar hierarchy of models is recovered, with the V20X model generally outperforming V20, which in turn generally outperforms V15. The errors peak for all models in the summer, again due to the lakes not being fully mixed. There is also an uptick in the prediction error for all models during the winter when the freezing is greatest - this indicates how ice cover can strongly influence the land surface temperature response. LST response. The familiar hierarchy of models is recovered; VESPER V15 is generally outperformed by the more updated models. In turn VESPER V20X is a general improvement over VESPER V20 throughout the year, especially during the winter months where the training noise is minimal. Since this is the time when freezing is greatest, this suggests that the additional monthly maps and salt lake maps are particularly useful during this time. For the southern hemisphere the story is different. The errors are smallest during the middle of the year when we expect the freezing to be greatest. During the spring and autumn the errors are largest - this is correlated with a decrease in the number of observations suggesting that this is due to poorer data quality due to cloud cover. In the summer when the weather is clearer the errors start to decrease again. Given this variation in the data quality due to cloud cover it is difficult to draw any strong conclusions, and again for stronger performance cloud independent data should be used. What is obvious for the southern hemisphere glacier grid points is that the VESPER V20 and VESPER V20X models struggle to improve on VESPER V15, unlike in the northern hemisphere. This suggests that the updated V20 fields are still insufficiently accurate for southern latitudes.

Mean prediction error in the surface temperature  $\bar{\Delta}K$ , averaged over all grid points, for each of the 3 models over the course of the test year for (top panel) Lake Updates, (second panel) Lake-Ground Updates, (third panel) Vegetation Updates, (fourth panel) Glacier Updates, northern hemisphere and (bottom panel) Glacier Updates, southern hemisphere. For the Glacier Updates category we again exclude grid points where the number of MODIS observations per ERA data point is less than 50. For the Lake categories, all models follow the same general profile, with the V20X model generally outperforming the V20 model over the year, which in turn outperforms the V15 model. The value of the additional V20 correction fields and the V20X monthly lake maps and salt lake maps, is evident.

We have also discussed previously particular grid points where there is expected to be that will likely show a large degree of temporal variability, or the lakes are saline, and as a

consequence the static physiographic V15/V20 fields struggle to make accurate predictions (e.g. Table 225). In Figure 16 we present timeseries for two of these points: Lake Natron in Tanzania and Gujarat Province, India the Great Salt Lake Desert, Utah and Chott Felhrir, Algeria. Both these points were discussed in Sections ?? and ??3.1.1, 3.2.1. We can see that for these two selected points the hierarchy of models no longer holds. Whilst there is a large degree of variability, and there is no clear separation between models that we get when averaging over all grid points as in Fig 15 for some parts of the year, generally it can be seen that VESPER\_V20 performs worse than VESPER\_V15. For the Great Salt Lake the inaccuracy when using the V20 model performs the worst, indicating that the updated fields are not accurate in these regions. For Lake Natron the physiographic fields is most pronounced during the summer months. April, May and June are some of the wettest months in this region. But the updated V20 /V20X models are significantly worse throughout almost the entire year. The updated models which fields specify a much larger smaller lake fraction than in V15 – perform well at the beginning and start of the year which tend to be the wettest months at Lake Natron. However, during the summer as the lake dries out the errors grow significantly (~ 0.5 compared to 0.0). Consequently during this time the V20 fields are maximally inaccurate and the prediction error of the VESPER\_V20 model grows accordingly. This indicates again that the updated V20 fields are in fact over-corrections for this area. Similarly, whilst the V15X model is a significant improvement over V20/The inclusion of monthly lake maps and salt lake maps in VESPER\_V20X – since it does not have these inaccurate fields – it is still less performant than the basic V15 again due to the additional water that V15X specifies. Together this strongly indicates that there is little surface water at Lake Natron during 2019.

For Gujarat Province in Northern India the story is different. Now the notably reduces the error during these summer months. For Algeria, we can see that VESPER\_V20 model is systematically worse than underperforms VESPER\_V15 over throughout the entire year, indicating that the static For this grid point the lake was completely removed when updating the V20 fields are less accurate than the V15 fields. The with the lake fraction reducing from ~ 0.35 to 0.0. This also appears to have been an over-correction. The separation between the models is most pronounced in the early months of the year; in the winter months both the prediction error and the variance increase - this period is the wet season in Algeria where the wadi which feed Chott Felhrir fill up. Similar to the Great Salt Lake Desert, the inclusion of the monthly lake maps in VESPER\_V20X model shows a strong time variability, with the errors being smallest in the summer which is the wet season in Gujarat and largest in the winter which is the dry season. This suggests that the monthly maps are most accurate during

the summer, providing extra information which is missing from V15/ improves the prediction accuracy, most notably in the early months of the year. Again, later in the year the training noise is much greater and so it is harder to separate the predictions of the model, but on average VESPER\_V20X outperforms VESPER\_V20, but may be overestimates during the winter. The V15X model has a notably strong performance, outperforming the other models almost every month. This again is further evidence of the inaccuracy of the V20 fields and the value of the time-variable monthly water information over the entire year, highlighting the value of these additional physiographic fields. monthly fields.

## 4 Discussion

We have seen how VESPER can quantitatively evaluate the value of updates to the lake surface parametrisation as well as identifying areas where the updates are insufficiently accurate. For the former VESPER was able to show that the major regions where the lake surface parametrisation fields were updated - such as the Aral sea - enjoyed more accurate predictions, which verifies both the accuracy of the fields and their information content with respect to predicting skin temperatures. For the latter VESPER was able to identify grid points where the predictions became worse with the updated fields, indicating that the updated fields were in fact less accurate. More generally we have also seen how detailed knowledge of surface water fields (e.g. up to date permanent water distribution, seasonal water distribution, salt lake distribution, etc.) can notably improve the accuracy with which the skin temperature can be modelled, e.g. grid points with significant updates (i.e. where the field has changed by  $\geq 10\%$ ) to the lake fields show a mean absolute error reduction of skin temperature globally of 0.450.37K (Table ??). Given the performance of VESPER it may be possible in the future to update or correct the input fields at a high cadence, e.g. yearly or even more frequently.

There are multiple possible further extensions of this work. We have not currently included the errors on the MODIS observations into the VESPER model. During the “matching-in-space” step relating the ERA and MODIS data (Section 2.3.2), it could be a worthwhile extension to weight the averaged MODIS points by their corresponding errors (e.g. Fig. ??5b) when deriving a single MODIS observation for a given ERA grid point. This would then provide a more accurate and confident representation of the true surface temperature at a particular space-time point. Due to the inherent stochasticity of training a model it is also possible for different models to settle in different local minimas i. e. the network variance. If we have seen that some grid points have a particularly large training noise. To better quantify this effect and try to draw stronger conclusions

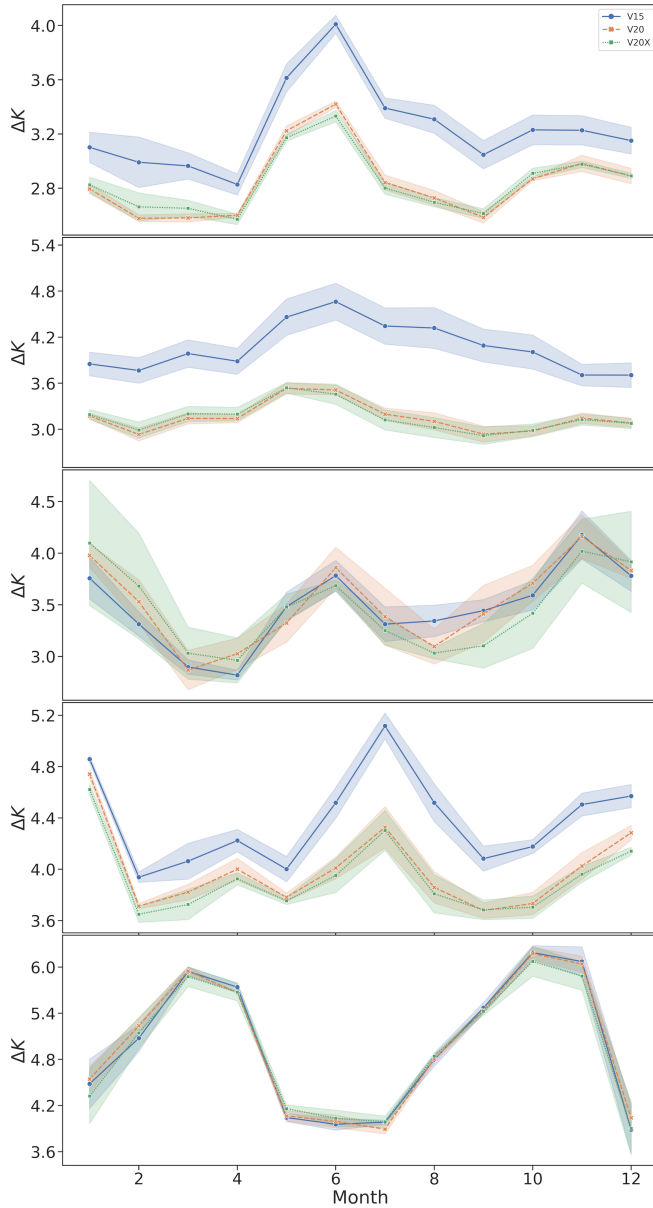


**Figure 15.** Variation in the Mean prediction error for in the surface temperature  $\Delta K$ , averaged over all grid points at, for each of the 3 models over the course of the test year for (top panel) Lake Natron Updates, Tanzania (top panel second panel) and Gujarat Province Lake-Ground Updates, India (bottom panel third panel) – There is a large degree of variability Vegetation Updates, but for (fourth panel) Glacier Updates, northern hemisphere and (bottom panel) Glacier Updates, southern hemisphere. The shaded regions show the  $1\sigma$  training noises. For the Lake Natron categories, all models follow the same general profile, with the VESPER V20 and VESPER V20X models are generally less performant than outperforming VESPER V15 and V15X, indicating that model over the updated V20 fields are less accurate here year. The augmented models with saline and monthly lake maps outperform those without, indicating the value of these fields in these regions.

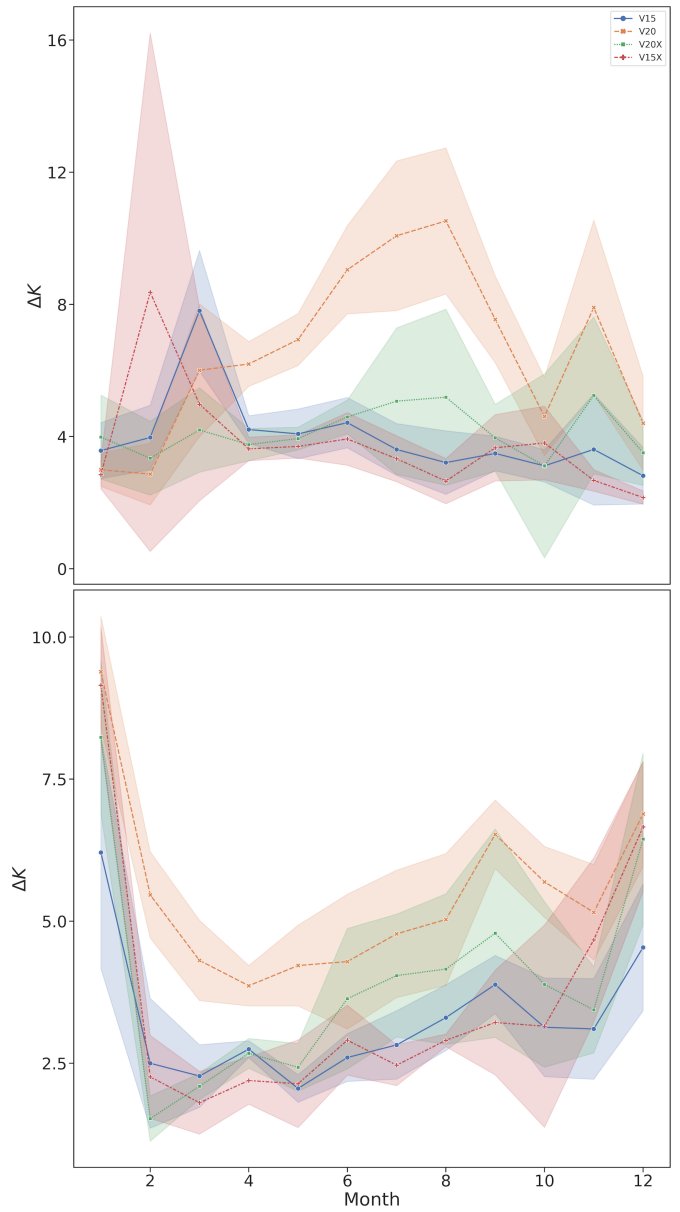


**Figure 16.** Variation in the prediction error for the grid points at Great Salt Lake, Utah (top panel) and Chott Felhrir, Algeria (bottom panel). There is a large degree of variability, but for both grid points VESPER V20 model is generally less performant than VESPER V15, indicating that the updated V20 fields are less accurate here. Corrections introduced by the augmented VESPER V20X model with saline and monthly lake maps outperform those without, indicating the value of these fields in these regions. The shaded regions show the  $1\sigma$  training noises.

for this subset of points it would also be desirable to train an ensemble of models ("ensemble learning") and combine the predictions from multiple models to reduce this variance. Additionally, our examination of the value of the monthly lake maps is only a preliminary study. It would be of interest to follow seasonal lakes over a longer time period (e.g. decadal) beyond the 12 month maps that we use, in order to better quantify their time variability, as well as the differences between years (e.g. if the lake fraction was particularly high in the January of one year, but low in the subsequent year). It would also be of interest to try to quantify if VESPER and ECLand respond to changes in the input parametrisations in the same way, which is key to be able to then apply the VESPER results to the full earth system model development. Since VESPER is trained on ERA5, if we want to model the outputs of the IFS we must assume that the statistical behaviour of the input fields does not change from ERA to IFS. This is a fair assumption, but it would be interesting to investigate this quantitatively in greater detail. We have focused here primarily on hydrological applications, our primary concern being the ability to evaluate the parametrised water body representation, however the method would work generally for any updated fields that we want to assess could also be explored. Extension to non-lake hydrological fields like wetland extant extent or river bathymetry model parameters, or even non hydrological fields such as orography would be an interesting further development. The development of a more mature, integrated pipeline for automatically evaluating updated parametrisations could also be a worthwhile pursuit. Another natural-

Another natural and interesting extension of this work would be to use VESPER to perform a feature importance or sensitivity analysis for the various input fields of the neural network. Additionally, an approach which may prove fruitful in the enterprise for improved parametrised representation of water bodies is to invert the problem and treat VESPER as a function to optimise. That is to say, VESPER can be thought of as a function which takes some inputs - in this case a lake parametrisation - and returns a loss metric i.e. how accurate the predictions are compared to the test set. Given this loss metric it may then be possible to vary the inputs and use standard optimisation techniques to learn the optimal parametrisation. Whilst this may be an expensive technique as there are effectively two nested models over which to optimise (for every optimisation step in the higher model, one must train the VESPER network from scratch) it could be possible given appropriate hardware or with reduced data focusing just on targeted locations (e.g. "What is the best way to represent the lakes in this area?" "What is the best way to represent the lakes in this area?"). The loss gradient information can also be used to tune individual features, informing whether an input variable should be larger or smaller.

## 5 Conclusion

Weather and climate modelling rely on accurate, up-to-date descriptions of surface fields, such as inland water, so as to provide appropriate boundary conditions for the numerical evolution. Lakes can significantly influence both weather and climate, but sufficiently accurate representation of lakes is challenging and the natural changes in water bodies mean that these representations need to be frequently updated. A new method based on a neural network regressor for automatically and quickly verifying the updated lake fields - VESPER - has been presented in this work. This tool has been deployed to verify the recent updates to the FLake parametrisation, which include additional datasets such as the GSWE and updated methods for determining the lake depth from GLDBv3. The updated parametrisation fields were shown globally to be an improvement over the original fields; for a subset of grid points which have had significant updates to the lake fields, the prediction error in the skin temperature decreased by 0.45a MAE of 0.37K. Conversely, VESPER also identified individual grid points where the updated lake fields were less accurate, enabling these points to subsequently be corrected, such as incorrect removal of lake water and losing forests to bare ground leading to errors of 1.1K. Multiple further extensions of this work, including extension to non lake fields and the development of a more mature integrated pipeline have been discussed.

## 6 Code

The code used in constructing VESPER, including the methods for joining the ERA and MODIS datasets and the construction of the neural network regression model is open-sourced at

## 6 Acknowledgments

This project has received funding from the European Research Council (ERC) under the European Union's Horizon 2020 research and innovation programme (Grant No 741112).

*Code availability.* The code used in constructing VESPER, including the methods for joining the ERA and MODIS datasets and the construction of the neural network regression model is open-sourced at <https://github.com/tomkimpson/ML4L>

*Author contributions.* All the authors contributed equally to the work. Tom Kimpson wrote the manuscript with contributions from all other authors.

*Competing interests.* The authors declare that they have no conflict of interest.

*Acknowledgements.* This project has received funding from the European Research Council (ERC) under the European Union's Horizon 2020 research and innovation programme (Grant No 741112). PD gratefully acknowledges funding from the ESiWACE project funded under Horizon 2020 No. 823988. PD and MC gratefully acknowledge funding from the MAELSTROM EuroHPC-JU project (JU) under No 955513. The JU receives support from the European Union's Horizon research and innovation programme and United Kingdom, Germany, Italy, Luxembourg, Switzerland, and Norway.

## References

Two Decades of Change at Toshka Lakes, <https://earthobservatory.nasa.gov/images/149334/two-decades-of-change-at-toshka-lakes>, accessed: 2022-09-30.

Abadi, M., Agarwal, A., Barham, P., Brevdo, E., Chen, Z., Citro, C., Corrado, G. S., Davis, A., Dean, J., Devin, M., Ghemawat, S., Goodfellow, I., Harp, A., Irving, G., Isard, M., Jia, Y., Jozefowicz, R., Kaiser, L., Kudlur, M., Levenberg, J., Mané, D., Monga, R., Moore, S., Murray, D., Olah, C., Schuster, M., Shlens, J., Steiner, B., Sutskever, I., Talwar, K., Tucker, P., Vanhoucke, V., Vasudevan, V., Viégas, F., Vinyals, O., Warden, P., Wattenberg, M., Wicke, M., Yu, Y., and Zheng, X.: TensorFlow: Large-Scale Machine Learning on Heterogeneous Systems, <https://www.tensorflow.org/>, software available from tensorflow.org, 2015.

Abadi, M., Agarwal, A., Barham, P., Brevdo, E., Chen, Z., Citro, C., Corrado, G. S., Davis, A., Dean, J., Devin, M., Ghemawat, S., Goodfellow, I., Harp, A., Irving, G., Isard, M., Jia, Y., Jozefowicz, R., Kaiser, L., Kudlur, M., Levenberg, J., Mane, D., Monga, R., Moore, S., Murray, D., Olah, C.,

Schuster, M., Shlens, J., Steiner, B., Sutskever, I., Talwar, K., Tucker, P., Vanhoucke, V., Vasudevan, V., Viegas, F., Vinyals, O., Warden, P., Wattenberg, M., Wicke, M., Yu, Y., and Zheng, X.: TensorFlow: Large-Scale Machine Learning on Heterogeneous Distributed Systems, arXiv e-prints, arXiv:1603.04467, <https://doi.org/10.48550/arXiv.1603.04467>, 2016.

Amante, C. and Eakins, B. W.: ETOPO1 Global Relief Model converted to PanMap layer format, <https://doi.org/10.1594/PANGAEA.769615>, 2009.

Arino, O., Ramos Perez, J. J., Kalogirou, V., Bontemps, S., Defourny, P., and Van Bogaert, E.: Global Land Cover Map for 2009 (GlobCover 2009), <https://doi.org/10.1594/PANGAEA.787668>, 2012.

Bischl, B., Binder, M., Lang, M., Pielok, T., Richter, J., Coors, S., Thomas, J., Ullmann, T., Becker, M., Boulesteix, A.-L., Deng, D., and Lindauer, M.: Hyperparameter Optimization: Foundations, Algorithms, Best Practices and Open Challenges, arXiv e-prints, arXiv:2107.05847, 2021.

Bontemps, S., Defourny, P., Van Bogaert, E., Arino, O., Kalogirou, V., and Ramos Perez, J.: GLOBCOVER 2009 Product description and validation report, [http://due.esrin.esa.int/page\\_globcover.php](http://due.esrin.esa.int/page_globcover.php), accessed: 2022-06-01, 2011.

Boussetta, S., Balsamo, G., Arduini, G., Dutra, E., McNorton, J., Choulga, M., Agustí-Panareda, A., Beljaars, A., Wedi, N., Muñoz-Sabater, J., de Rosnay, P., Sandu, I., Hadade, I., Carver, G., Mazzetti, C., Prudhomme, C., Yamazaki, D., and Zsoter, E.: ECLand: The ECMWF Land Surface Modelling System, Atmosphere, 12, <https://doi.org/10.3390/atmos12060723>, 2021.

Chantry, M., Hatfield, S., Duben, P., Polichtchouk, I., and Palmer, T.: Machine learning emulation of gravity wave drag in numerical weather forecasting, in: EGU General Assembly Conference Abstracts, EGU General Assembly Conference Abstracts, pp. EGU21-7678, <https://doi.org/10.5194/egusphere-egu21-7678>, 2021.

Choulga, M., Kourzeneva, E., Zakharova, E., and Doganovsky, A.: Estimation of the mean depth of boreal lakes for use in numerical weather prediction and climate modelling, Tellus A: Dynamic Meteorology and Oceanography, 66, 21 295, <https://doi.org/10.3402/tellusa.v66.21295>, 2014.

Choulga, M., Kourzeneva, E., Balsamo, G., Boussetta, S., and Wedi, N.: Upgraded global mapping information for earth system modelling: an application to surface water depth at the ECMWF, Hydrology and Earth System Sciences, 23, 4051–4076, <https://doi.org/10.5194/hess-23-4051-2019>, 2019.

DelSontro, T., Beaulieu, J. J., and Downing, J. A.: Greenhouse gas emissions from lakes and impoundments: Upscaling in the face of global change, Limnology and Oceanography Letters, 3, 64–75, <https://doi.org/https://doi.org/10.1002/lol2.10073>, 2018.

Duan, S.-B., Li, Z.-L., Li, H., Götsche, F.-M., Wu, H., Zhao, W., Leng, P., Zhang, X., and Coll, C.: Validation of Collection 6 MODIS land surface temperature product using in situ measurements, Remote Sensing of Environment, 225, 16–29, <https://doi.org/https://doi.org/10.1016/j.rse.2019.02.020>, 2019.

Düben, P., Modigliani, U., Geer, A., Siemen, S., Pappenberger, F., Bauer, P., Brown, A., Palkovic, M., Raoult, B., Wedi, N., and Baousis, V.: Machine learning at ECMWF: A roadmap for the next 10 years, <https://doi.org/10.21957/ge7ckgm>, 2021.

ECMWF: IFS Documentation: CY47R3 – Part IV: Physical processes, <https://doi.org/https://doi.org/10.21957/eyrpir4vj>, 2021.

Eerola, K., Rontu, L., Kourzeneva, E., Pour, H. K., and Duguay, C.: Impact of partly ice-free Lake Ladoga on temperature and cloudiness in an anticyclonic winter situation – a case study using a limited area model, *Tellus A: Dynamic Meteorology and Oceanography*, 66, 23 929, <https://doi.org/10.3402/tellusa.v66.23929>, 2014.

FAO, U.: Digital soil map of the world and derived soil properties, 2003.

Franz, D., Mammarella, I., Boike, J., Kirillin, G., Vesala, T., Bornemann, N., Larmanou, E., Langer, M., and Sachs, T.: Lake-Atmosphere Heat Flux Dynamics of a Thermokarst Lake in Arctic Siberia, *Journal of Geophysical Research: Atmospheres*, 123, 5222–5239, <https://doi.org/10.1029/2017JD027751>, 2018.

Freire, S., MacManus, K., Pesaresi, M., Doxsey-Whitfield, E., and Mills, J.: Development of new open and free multi-temporal global population grids at 250 m resolution, AGILE, [https://agile-online.org/Conference\\_Paper/cds/agile\\_2016/shortpapers/152\\_Paper\\_in\\_PDF.pdf](https://agile-online.org/Conference_Paper/cds/agile_2016/shortpapers/152_Paper_in_PDF.pdf), 2016.

GLIMS and NSIDC: Global Land Ice Measurements from Space glacier database, <https://doi.org/DOI:10.7265/N5V98602>, compiled and made available by the international GLIMS community and the National Snow and Ice Data Center, 2005, updated 2018.

GSFC, N.: MODIS, <https://modis.gsfc.nasa.gov/>, accessed: 2022-06-01.

Hatfield, S., Chantry, M., Dueben, P., Lopez, P., Geer, A., and Palmer, T.: Building Tangent-Linear and Adjoint Models for Data Assimilation With Neural Networks, *Journal of Advances in Modeling Earth Systems*, 13, e02521, <https://doi.org/10.1029/2021MS002521>, 2021.

Hersbach, H., Bell, B., Berrisford, P., Hirahara, S., Horányi, A., Muñoz-Sabater, J., Nicolas, J., Peubey, C., Radu, R., Schepers, D., Simmons, A., Soci, C., Abdalla, S., Abellán, X., Balsamo, G., Bechtold, P., Biavati, G., Bidlot, J., Bonavita, M., De Chiara, G., Dahlgren, P., Dee, D., Diamantakis, M., Dragani, R., Flemming, J., Forbes, R., Fuentes, M., Geer, A., Haimberger, L., Healy, S., Hogan, R. J., Hólm, E., Janisková, M., Keeley, S., Laloyaux, P., Lopez, P., Lupu, C., Radnoti, G., de Rosnay, P., Rozum, I., Vamborg, F., Villaume, S., and Thépaut, J.-N.: The ERA5 global reanalysis, *Quarterly Journal of the Royal Meteorological Society*, 146, 1999–2049, <https://doi.org/10.1002/qj.3803>, 2020.

Hewson, T. D. and Pillou, F. M.: A low-cost post-processing technique improves weather forecasts around the world, *Communications Earth and Environment*, 2, 132, <https://doi.org/10.1038/s43247-021-00185-9>, 2021.

Howat, I. M., Negrete, A., and Smith, B. E.: The Greenland Ice Mapping Project (GIMP) land classification and surface elevation data sets, *The Cryosphere*, 8, 1509–1518, <https://doi.org/10.5194/tc-8-1509-2014>, 2014.

Huang, W., Cheng, B., Zhang, J., Zhang, Z., Vihma, T., Li, Z., and Niu, F.: Modeling experiments on seasonal lake ice mass and energy balance in the Qinghai–Tibet Plateau: a case study, *Hydrology and Earth System Sciences*, 23, 2173–2186, <https://doi.org/10.5194/hess-23-2173-2019>, 2019.

Johannsen, F., Ermida, S., Martins, J. P. A., Trigo, I. F., Nogueira, M., and Dutra, E.: Cold Bias of ERA5 Summertime Daily Maximum Land Surface Temperature over Iberian Peninsula, *Remote Sensing*, 11, <https://doi.org/10.3390/rs11212570>, 2019.

Kingma, D. P. and Ba, J.: Adam: A Method for Stochastic Optimization, *arXiv e-prints*, arXiv:1412.6980, 2014.

Kourzeneva, E., Asensio, H., Martin, E., and Faroux, S.: Global gridded dataset of lake coverage and lake depth for use in numerical weather prediction and climate modelling, *Tellus A: Dynamic Meteorology and Oceanography*, 64, 15 640, <https://doi.org/10.3402/tellusa.v64i0.15640>, 2012.

Liu, H., Jezek, K., Li, B., and Zhao, Z.: Radarsat Antarctic Mapping Project Digital Elevation Model, Version 2, <https://doi.org/10.5067/8JKNEW6BFRVD>, 2015.

Lu, P., Cao, X., Li, G., Huang, W., Leppäranta, M., Arvola, L., Huotari, J., and Li, Z.: Mass and Heat Balance of a Lake Ice Cover in the Central Asian Arid Climate Zone, *Water*, 12, 2888, <https://doi.org/10.3390/w12102888>, 2020.

Mironov, D. V.: Parameterization of lakes in numerical weather prediction: Description of a lake model, DWD Offenbach, Germany, 2008.

Molnia, B. F. and Post, A.: Surges of the Bering Glacier, in: *Bering Glacier: Interdisciplinary Studies of Earth's Largest Temperate Surging Glacier*, Geological Society of America, [https://doi.org/10.1130/2010.2462\(15\)2010](https://doi.org/10.1130/2010.2462(15)2010), 2010.

Muñoz Sabater, J., Dutra, E., Agustí-Panareda, A., Albergel, C., Arduini, G., Balsamo, G., Boussetta, S., Choulga, M., Harrigan, S., Hersbach, H., Martens, B., Miralles, D. G., Piles, M., Rodríguez-Fernández, N. J., Zsoter, E., Buontempo, C., and Thépaut, J.-N.: ERA5-Land: a state-of-the-art global reanalysis dataset for land applications, *Earth System Science Data*, 13, 4349–4383, <https://doi.org/10.5194/essd-13-4349-2021>, 2021a.

Muñoz Sabater, J., Dutra, E., Agustí-Panareda, A., Albergel, C., Arduini, G., Balsamo, G., Boussetta, S., Choulga, M., Harrigan, S., Hersbach, H., Martens, B., Miralles, D. G., Piles, M., Rodríguez-Fernández, N. J., Zsoter, E., Buontempo, C., and Thépaut, J.-N.: ERA5-Land: a state-of-the-art global reanalysis dataset for land applications, *Earth System Science Data*, 13, 4349–4383, <https://doi.org/10.5194/essd-13-4349-2021>, 2021b.

Munoz Sabater, J.: ERA5-Land hourly data from 1981 to present., <https://doi.org/10.24381/cds.e2161bac>, 2019.

Notaro, M., Zarrin, A., Vavrus, S., and Bennington, V.: Simulation of Heavy Lake-Effect Snowstorms across the Great Lakes Basin by RegCM4: Synoptic Climatology and Variability, *Monthly Weather Review*, 141, 1990 – 2014, <https://doi.org/10.1175/MWR-D-11-00369.1>, 2013.

Pace, M. and Prairie, Y.: Respiration in lakes, *Respiration in Aquatic Ecosystems*, <https://doi.org/10.1093/acprof:oso/9780198527084.003.0007>, 2005.

Parkinson, C.: Aqua: An Earth-Observing Satellite Mission to Examine Water and Other Climate Variables, *Geoscience and Remote Sensing, IEEE Transactions on*, 41, 173 – 183, <https://doi.org/10.1109/TGRS.2002.808319>, 2003.

Pekel, J.-F., Cottam, A., Gorelick, N., and Belward, A.: High-resolution mapping of global surface water and its long-term changes, *Nature*, 540, <https://doi.org/10.1038/nature20584>, 2016.

RAPIDS: cuML - GPU Machine Learning Algorithms, <https://github.com/rapidsai/cuml>, v22.04.00.

Saunois, M., Stavert, A. R., Poulter, B., Bousquet, P., Canadell, J. G., Jackson, R. B., Raymond, P. A., Dlugokencky, E. J., Houweling, S., Patra, P. K., Ciais, P., Arora, V. K., Bastviken, D., and Tans, P. P.: Global atmospheric methane from 1984 to 2018, *Science*, 367, 1220190, <https://doi.org/10.1126/science.1220190>, 2020.

D., Bergamaschi, P., Blake, D. R., Brailsford, G., Bruhwiler, L., Carlson, K. M., Carroll, M., Castaldi, S., Chandra, N., Crevoisier, C., Crill, P. M., Covey, K., Curry, C. L., Etiopic, G., Frankenberg, C., Gedney, N., Hegglin, M. I., Höglund-Isaksson, L., Hugelius, G., Ishizawa, M., Ito, A., Janssens-Maenhout, G., Jensen, K. M., Joos, F., Kleinen, T., Krummel, P. B., Langenfelds, R. L., Laruelle, G. G., Liu, L., Machida, T., Maksyutov, S., McDonald, K. C., McNorton, J., Miller, P. A., Melton, J. R., Morino, I., Müller, J., Murguia-Flores, F., Naik, V., Niwa, Y., Noce, S., O'Doherty, S., Parker, R. J., Peng, C., Peng, S., Peters, G. P., Prigent, C., Prinn, R., Ramonet, M., Regnier, P., Riley, W. J., Rosentreter, J. A., Segers, A., Simpson, I. J., Shi, H., Smith, S. J., Steele, L. P., Thornton, B. F., Tian, H., Tohjima, Y., Tubiello, F. N., Tsuruta, A., Viovy, N., Voulgarakis, A., Weber, T. S., van Weele, M., van der Werf, G. R., Weiss, R. F., Worthy, D., Wunch, D., Yin, Y., Yoshida, Y., Zhang, W., Zhang, Z., Zhao, Y., Zheng, B., Zhu, Q., Zhu, Q., and Zhuang, Q.: The Global Methane Budget 2000–2017, *Earth System Science Data*, 12, 1561–1623, <https://doi.org/10.5194/essd-12-1561-2020>, 2020.

20 Schaaf, C. B., Gao, F., Strahler, A. H., Lucht, W., Li, X., Tsang, T., Strugnell, N. C., Zhang, X., Jin, Y., Muller, J.-P., Lewis, P., Barnsley, M., Hobson, P., Disney, M., Roberts, G., Dunderdale, M., Doll, C., d'Entremont, R. P., Hu, B., Liang, S., Privette, J. L., and Roy, D.: First operational BRDF, albedo nadir reflectance products from MODIS, *Remote Sensing of Environment*, 83, 135–148, [https://doi.org/https://doi.org/10.1016/S0034-4257\(02\)00091-3](https://doi.org/10.1016/S0034-4257(02)00091-3), the Moderate Resolution Imaging Spectroradiometer (MODIS): a new generation of Land Surface Monitoring, 2002.

25 Schiavina, M., Freire, S., and MacManus, K.: GHS-POP R2022A - GHS population grid multitemporal (1975–2030), [https://ghsl.jrc.ec.europa.eu/ghs\\_pop2022.php](https://ghsl.jrc.ec.europa.eu/ghs_pop2022.php), 2022.

30 Slater, T., Shepherd, A., McMillan, M., Muir, A., Gilbert, L., Hogg, A. E., Konrad, H., and Parrinello, T.: A new digital elevation model of Antarctica derived from CryoSat-2 altimetry, *The Cryosphere*, 12, 1551–1562, <https://doi.org/10.5194/tc-12-1551-2018>, 2018.

35 Thiery, W., Davin, E. L., Panitz, H.-J., Demuzere, M., Lhermitte, S., and van Lipzig, N.: The Impact of the African Great Lakes on the Regional Climate, *Journal of Climate*, 28, 4061 – 4085, <https://doi.org/10.1175/JCLI-D-14-00565.1>, 2015.

40 Thiery, W., Gudmundsson, L., Bedka, K., Semazzi, F. H. M., Lhermitte, S., Willems, P., van Lipzig, N. P. M., and Seneviratne, S. I.: Early warnings of hazardous thunderstorms over Lake Victoria, *Environmental Research Letters*, 12, 074012, <https://doi.org/10.1088/1748-9326/aa7521>, 2017.

45 Tranvik, L. J., Downing, J. A., Cotner, J. B., Loiselle, S. A., Striegl, R. G., Ballatore, T. J., Dillon, P., Finlay, K., Fortino, K., Knoll, L. B., Kortelainen, P. L., Kutser, T., Larsen, S., Laurion, I., Leech, D. M., McCallister, S. L., McKnight, D. M., Melack, J. M., Overholt, E., Porter, J. A., Prairie, Y., Renwick, W. H., Roland, F., Sherman, B. S., Schindler, D. W., Sobek, S., Tremblay, A., Vanni, M. J., Verschoor, A. M., von Wachenfeldt, E., and Weyhenmeyer, G. A.: Lakes and reservoirs as regulators of carbon cycling and climate, *Limnology and Oceanography*, 54, 2298–2314, [https://doi.org/https://doi.org/10.4319/lo.2009.54.6\\_part\\_2.2298](https://doi.org/https://doi.org/10.4319/lo.2009.54.6_part_2.2298), 2009.

50 Vavrus, S., Notaro, M., and Zarrin, A.: The Role of Ice Cover in Heavy Lake-Effect Snowstorms over the Great Lakes Basin as Simulated by RegCM4, *Monthly Weather Review*, 141, 148 – 165, <https://doi.org/10.1175/MWR-D-12-00107.1>, 2013.

55 Verpoorter, C., Kutser, T., Seekell, D. A., and Tranvik, L. J.: A global inventory of lakes based on high-resolution satellite imagery, *Geophysical Research Letters*, 41, 6396–6402, <https://doi.org/https://doi.org/10.1002/2014GL060641>, 2014.

60 Viterbo, P.: A review of parametrization schemes for land surface processes, <https://www.ecmwf.int/node/16960>, 2002.

65 Wan, Z. and Dozier, J.: A generalized split-window algorithm for retrieving land-surface temperature from space, *IEEE Transactions on Geoscience and Remote Sensing*, 34, 892–905, <https://doi.org/10.1109/36.508406>, 1996.

70 Wan, Z., Hook, S., and Hulley, G.: MODIS/Aqua Land Surface Temperature/Emissivity Daily L3 Global 1km SIN Grid V061 [Data set], <https://doi.org/10.5067/MODIS/MYD11A1.06>, accessed: 2022-06-01.

75 Wan, Z., Hook, S., and Hulley, G.: MYD11A1 MODIS/Aqua Land Surface Temperature/Emissivity Daily L3 Global 1km SIN Grid V006 [Data set], NASA EOSDIS Land Processes DAAC, <https://doi.org/https://doi.org/10.5067/MODIS/MYD11A1.006>, accessed: 2022-06-01, 2015.

80 Weatherall, P., Marks, K. M., Jakobsson, M., Schmitt, T., Tani, S., Arndt, J. E., Rovere, M., Chayes, D., Ferrini, V., and Wigley, R.: A new digital bathymetric model of the world's oceans, *Earth and Space Science*, 2, 331–345, <https://doi.org/https://doi.org/10.1002/2015EA000107>, 2015.

85 Yu, T. and Zhu, H.: Hyper-Parameter Optimization: A Review of Algorithms and Applications, *arXiv e-prints*, arXiv:2003.05689, 2020.